Comparison of ring-liner oil film thickness resulting from different injector designs in a diesel marine engine using an ultrasound measurement method

Rooke J, Li X, Brunskill H, Stark M and Dwyer-Joyce R,
SAE International Journal of Engines

Abstract

The global drive to combat climate change is a primary driving force towards producing greener and cleaner marine diesel engines to meet emission legislation. The main cause of an engine parasitic frictional loss is the interaction between piston rings and the cylinder liner. Therefore, the piston ring lubricating oil film has been the focus of much prior research chiefly focusing on small-scale automotive engines. This work employs the ultrasonic reflectometry technique to evaluate the oil film formation resulting from different lubricant injector arrangements on a large two-stroke marine diesel engine. A series of piezoelectric transducers close to top dead center have quantified the oil film thickness across three engine loading levels and three injector configurations. The injector configurations compare a more traditional pulse jet injector to a needle lift type injector which reduces the rate of lubricant atomization. The results gathered show the oil film thickness to increase with decreased engine load for all injector systems. The needle lift injector has been shown to increase the minimum oil film thickness for the first ring at top dead center, reducing the likelihood of boundary lubrication for this ring whilst also reducing the amount of lubricant present in the exhaust manifold.

Keywords

Diesel Marine Engine, Ultrasound, Oil film thickness, Piston ring

1 Introduction

Marine engines are the backbone of international shipping which has an essential role in enabling cost-effective world trade. The growth of this industry has led to greenhouse gas emissions from this sector alone being 2.2% of anthropogenic CO_2 emissions [1]. With a global drive to combat climate change, this highlights the need for novel technologies to be used in diesel marine engines to reduce emissions. This has led to the International Maritime Organization (IMO) implementing their initial strategy to reduce greenhouse gas emissions, aimed to reduce CO_2 emissions by at least 40% by 2030 relative to 2008 levels [1].

In an engine, 12% of the energy content of the fuel is wasted due to frictional losses, with 25% of those losses arising from the ring pack [2]. Therefore one methodology to lessen engine emissions is through enhanced understanding and control of the lubricating film between the piston rings and cylinder liner. Improved understanding of the lubricant mechanics between the piston rings and liner, enables the oil film thickness and oil injection rate to be optimized. Currently, lubricant oil thrown off into the combustion chamber causes 40-60% [3,4] of particulate emissions; this, therefore, has a major impact on engine efficiency and emissions.

The purpose of this study has been to establish a method to measure the oil film thickness between a piston ring and liner in a marine diesel engine and examine the effect of oil injector design. The RTX-6, a Winterthur Gas & Diesel test engine, was instrumented with ultrasonic transducers on the neutral side of a liner at a range of locations close to top dead center, TDC. Fired tests were run at a range of loads and oil feed rates for three lubricant injector systems to vary the lubricant presence on the liner.

2 Background

Over the past few decades techniques have been developed to measure the lubricating film between piston rings and the cylinder liner using its response to electromagnetism, light, or sound [5]. Research generally focuses on the area around TDC of the piston as the velocity is lower leading to an increased likelihood of oil film breakdown, metal-metal contact, and the region where greater oil throw-off occurs.

A common electrical approach is based upon the dielectric nature of the oil film as capacitance can be formed between two parallel electrodes of differing potentials, with the magnitude of the capacitance being proportional to the separation distance between the two. Through modifications to the liner, a capacitance probe can be mounted flush with the internal surface of the liner and the ring acts as the other electrode. This approach has measured oil films ranging from 0.2 to 9 μm [6-12] although the methodology is prone to breakdown from excessively thin films (< 1 μm) as shorting of the circuit may occur (metal-metal contact). A major assumption in this technique is that the region between the piston ring and liner is fully flooded with oil as cavitation changes the dielectric constant. This may alter the calculated oil film thickness value by up to a factor of two, therefore capacitance is more appropriate for minimum oil film thickness measurements.

Laser-induced fluorescence (LIF) is a frequently used optical approach based upon replacing a portion of the cylinder liner with a transparent window. This allows a laser to be shone through the window to the oil film, the photons excite electrons in the oil raising them to a higher energy state. On returning to their original energy state the electrons emit radiation of a smaller wavelength which can then be correlated to oil film thickness. LIF has previously measured oil films from 0.4 to 18 μm [9, 13-18] and has an improved spatial resolution relative to the capacitance method of an order of magnitude less than ring width. Furthermore, LIF can quantify the film thickness when the rings are not over the measurement region, providing a measure of residual oil levels.

The primary hindrance of both capacitance and LIF is the requirement of machining the liner through to the internal surface, either to mount a probe or to insert a transparent window. Major engine modifications are also prevalent in other techniques to quantify this oil film; resistance [19], strain gauge [20], and inductance [21,22]. This causes a fundamental change to one of the boundaries for the oil film and therefore has the potential to impact the film formation. An alternative technique is based upon ultrasonic reflectometry, where a piezoelectric transducer is mounted on the external surface of the liner and sound waves are pulsed through the liner with a partial reflection occurring from each boundary. The non-invasive nature of ultrasound overcomes the major flaw associated with both capacitance and laser-induced fluorescence. Previous automotive engine works have provided film thickness values ranging from 2 to 21 μm [5, 23-28]. The most comparable research to this work is on a Winterthur Gas & Diesel RTX-4 engine [29] where an ultrasonic transducer was instrumented onto the back surface of a piston ring to measure oil film thickness over the complete engine stroke. This work produced lubricant film thickness values down to a minimum of 6 μm. The transducer placement in this work, behind the piston ring, will have greatly increased complexity in routing wiring out of the engine. The spatial resolution of ultrasonic transducers is an area of concern as ultrasonic transducers provide an average measurement over the whole surface of the transducer, therefore the transducer width must be no greater than the ring width for representative results.

Once an ultrasonic wave is generated in a medium it propagates until it interacts with a discontinuity. For a wave that impacts perpendicular to a discontinuity, a partial transmittance/partial reflection of the wave occurs with the reflected portion being directed back towards the source of the wave. The magnitude of the reflected wave divided by that of the initial wave is termed the reflection coefficient, R, and is dependent on the stiffness between the two surfaces, see Equation 1, in which, z, is the acoustic impedance and is purely dependent on the speed of sound and density of the medium. The

reflected wave that propagates back to the source of the wave is the basis for ultrasonic reflectometry, see Figure 1 (a).

$$R = \frac{z_2 - z_1}{z_2 + z_1} \qquad 1$$

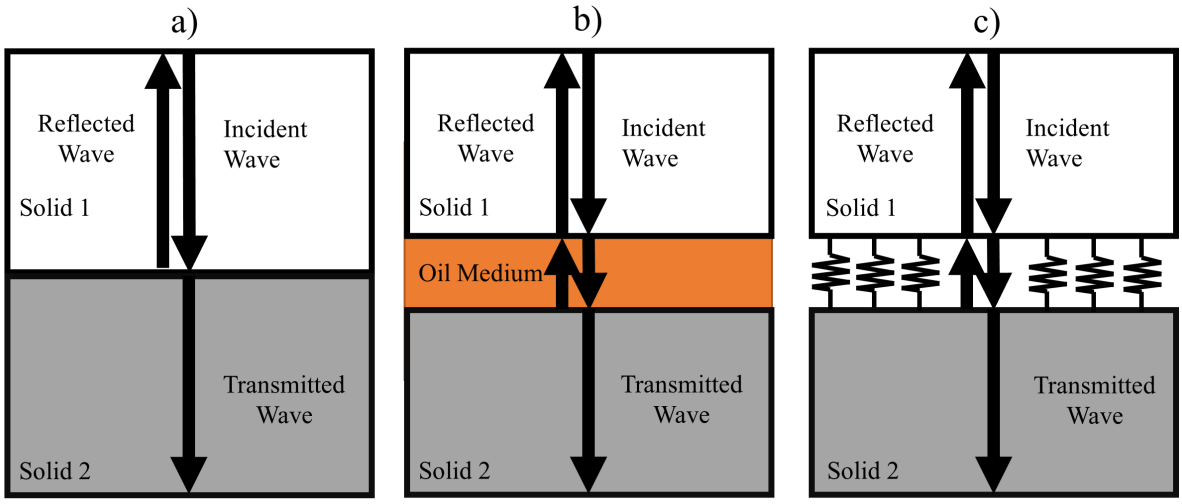

Figure 1 (a) Wave transmission between a solid-solid contact; (b) Wave transmission between a solid-oil-solid contact; (c) Equivalent solid-oil-solid contact following the Spring Model.

For two real engineering surfaces that are separated by an oil film (< 25 μm), as in Figure 1 (b), the system can be modeled using the Quasi-Static Spring Model as demonstrated by Schoenberg [30], see Figure 1 (c) and Equation 2. This is based on the two mediums being connected via a series of springs within their elastic region and the stiffness of the spring dictates the magnitude of the reflected portion of the wave. The interfacial stiffness, K, improves the model from being purely for two perfectly bonded materials into a real contact. The angular frequency of the ultrasonic signal is defined in ω and i indicates the complex terms in Equation 2.

$$R = \frac{z_2 - z_1 + \frac{i\omega z_1 z_2}{K}}{z_2 + z_1 + \frac{i\omega z_1 z_2}{K}} \qquad 2$$

The stiffness of the separating lubricant layer is based upon the liquid bulk modulus, B, and layer thickness, h, according to:

$$K = \frac{B}{h} \qquad 3$$

The bulk modulus of a fluid can be written in terms of the product of density, ρ, and speed of sound, c, squared, to give:

$$K = \frac{\rho c^2}{h} \qquad 4$$

The combination of Equations 2 and 4 gives an equation for the oil film thickness between a piston ring and liner [31]:

$$h = \frac{\rho c^2}{\omega z_1 z_2} \sqrt{\frac{|R^2|(z_2 + z_1)^2 - (z_2 - z_1)^2}{1 - R^2}} \qquad 5$$

3 Experimental Method

3.1 Test Engine

This work was performed on a two-stroke Winterthur Gas & Diesel RTX-6, see Figure 2, with some of the main engine parameters shown in Table 1. All three piston rings are barrel-faced single pieces of steel coated with chromium-ceramic.

Figure 2 A two-stroke Winterthur Gas & Diesel RTX-6 engine.

Table 1 Engine parameters.

Engine Parameter	Value
Max Power	6470 kW
Cylinder Bore	500 mm
Piston Stroke	2250 mm

The oil speed of sound and density has a major effect on the calculated oil film thickness (see Equation 5). To provide accurate measurements of the lubricating film, the temperature and pressure effects on oil speed of sound and density need to be considered. A series of experiments were performed to measure the speed of sound and density at a range of temperatures, T, and pressures, p. A regression curve fit was applied to the data to provide equations for the speed of sound and density as shown in Equations 6 and 7 respectively.

$$c = 0.0039T^2 - 3.39T + 4.13p + 1555.2 \quad (6)$$

$$\rho = 162.85 + \frac{888}{1 + 0.007(T - 20)} - \frac{5.88x10^4}{p + 3.61x10^2} \quad (7)$$

The piston stroke in a marine engine is significantly larger than its automotive counterpart, in the case of the RTX-6 engine the piston stroke is 2250 mm. To provide a lubricating film for the piston rings over the complete engine stroke two lubricant injector rails are required. The upper and lower injector

systems are located 400 mm and 800 mm from TDC of the piston, as shown in Figure 3. A complex control system is required to provide lubricant over the whole piston stroke. The standard lubricant distribution in this engine is to inject 80% of oil above the ring pack, 10% into, and 10% below the ring pack.

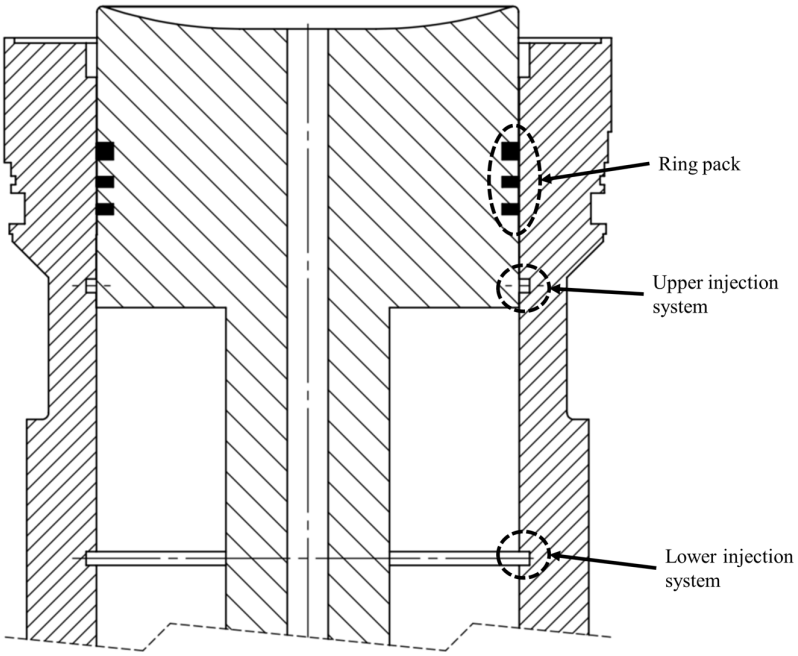

Figure 3 Lubricant injection rail locations with the piston at TDC.

In this study two different injector designs were tested, pulse jet (PJ) injectors and needle lift type (NLT) injectors. PJ injectors are a more traditional technique implemented in marine engines. This system consists of the lubricant oil injectors, lubricant tank, filter system, and lubricant oil dosage pumps, the lubricant system's main components and a schematic of the injector system is shown in Figure 4 (a) and (b) respectively. The dosage pump delivers lubricant to the injectors, powered by pressurized servo oil from the engine's oil circuit. The lube oil feed rate and timing are electronically controlled by a solenoid valve in the dosage pump, providing full flexibility in setting the injection timing over the full load range of the engine.

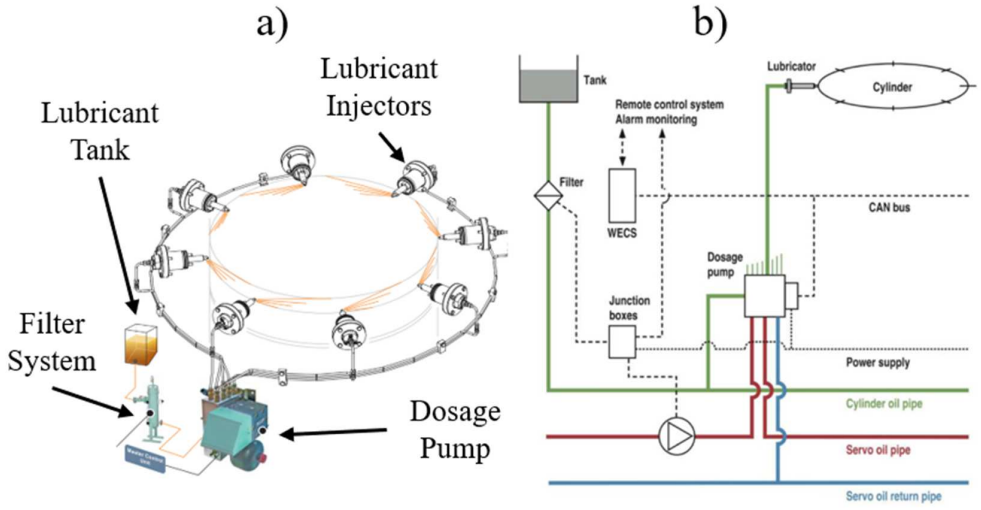

Figure 4 Pulse jet injector oil system. (a) Pulse jet injector components; (b) Schematic of the complete system [29].

A shortcoming of the PJ injector system is found in significant variations of the lubricant spray pattern. The necessity to control the spray characteristics, to optimize lubricant utilization leads to the development of a needle lift type injection system in conjunction with a common rail approach. NLT injectors are a prototype design that reduces lubricant atomization and thus provides greater control over lubricant consumption, relative to PJ injectors. The NLT injection system is shown in Figure 5.

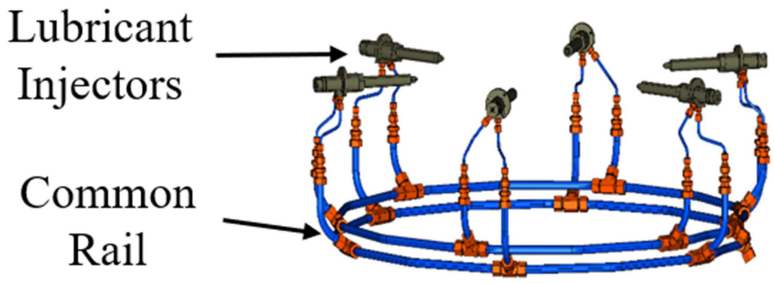

Figure 5 Needle lift type injectors.

These two injection systems were used to make up three injector configurations as shown in Table 2. In Configuration-3, the lower lubricant injection system consisted of modified PJ injectors to provide a more comparable injector nozzle design to NLT injectors.

Table 2 Injector setup summary.

Testing Configuration	Cylinder Injector System	Injector Type
Configuration-1	Upper System	PJ
	Lower System	NLT
Configuration-2	Upper System	NLT
	Lower System	PJ
Configuration-3	Upper System	PJ
	Lower System	PJ - Modified

3.2 Instrumentation

This work used four 1 MHz piezoelectric transducers for oil film thickness measurements with a 14 mm active element diameter that were manufactured by Saiboruixin Co. The sensors were coupled to the external surface of the liner by applying an industrial adhesive and curing overnight at room temperature. Limitations in access to the liner external surface caused the instrumentation to be restricted to the neutral side of the end cylinder of the RTX-6. To avoid any transducer being aligned with a cooling channel within the liner, the sensors were positioned at a series of locations on the liner centered around the neutral axis of the engine, as shown in Figure 6 (a). Critically, no modifications were made to the engine to perform this work.

One transducer was aligned with each piston ring (first ring, second ring, and third ring) when at their respective TDC positions. Whilst the fourth transducer was positioned between the top two rings at TDC, as shown in Figure 6 (b). Each transducer was circular, with the active element diameter less than the thickness of the piston rings; minimizing the averaging effect of piezoelectric transducers when the rings were at TDC. The crank angle corresponding to each piston ring being aligned with a transducer is summarised in Table 3.

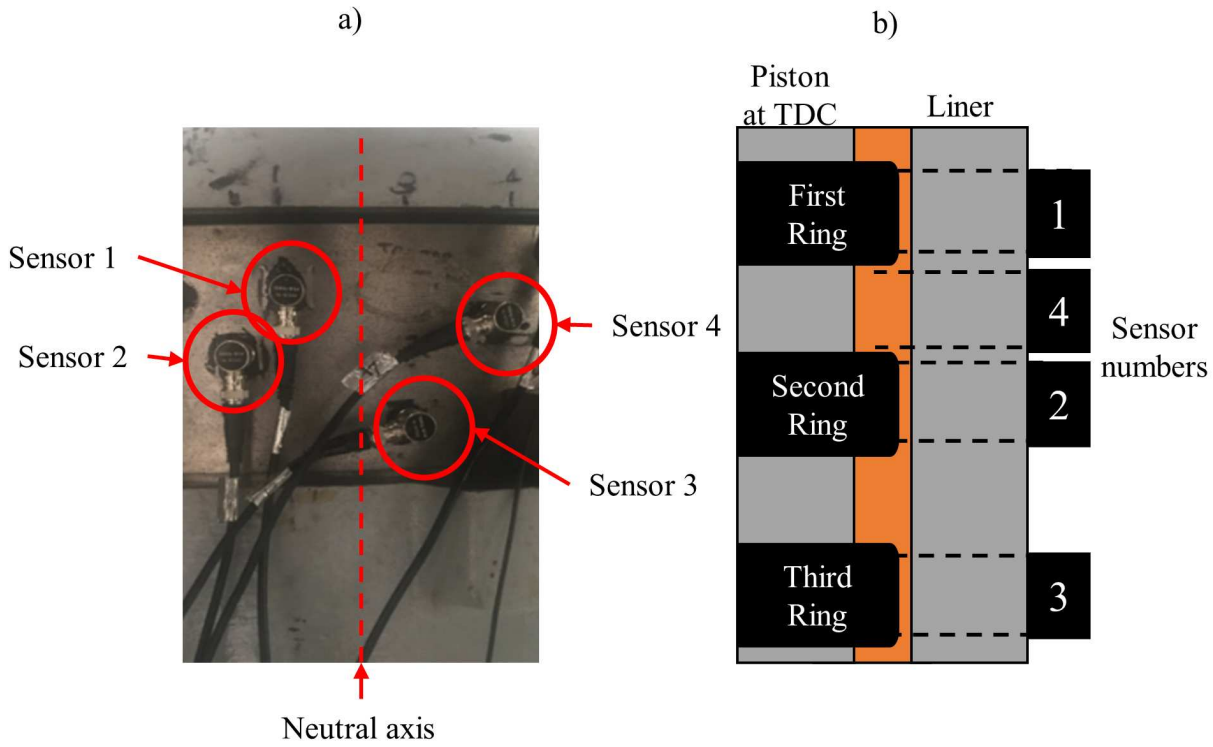

Figure 6 (a) Transducers instrumented onto the external surface of the liner; (b) Summary of transducer locations with the piston at TDC including transducer numbering convention.

Table 3 Crank angle alignment regions between ultrasonic transducer and piston ring.

Sensor	Ring	Piston ring alignment crank angle (°aTDC)
1	First	-8.5° to 8.5°
	Second	-
	Third	-
2	First	-15.6° to -9.9° 9.9° to 15.6°
	Second	-8° to 8°
	Third	-
3	First	-21° to -17.1° 17.1° to 21°
	Second	-16° to -11° 11° to 16°
	Third	-9.2° to 9.2°
4	First	-12.6° to -3.5° 3.5° to 12.6°
	Second	-
	Third	-

An ultrasonic pulser receiver, UPR, was used to manage the ultrasonic signals. The UPR consists of a card to generate short voltage pulses. These pulses were sent to the piezoelectric transducers which converted them to mechanical displacements, producing a pressure wave in the liner. The wave generated traveled through the liner which reflected from the oil film and was received by the same transducer. The transducer converted the mechanical displacement back to a voltage, which was recorded by a digitizer card in the UPR. The recorded data was a time-domain reflection of the ultrasonic wave, termed an A-Scan. Figure 7 shows a typical A-Scan with annotations corresponding

to the various signal features. The ultrasonic wave propagates through the liner reflecting from each boundary until the energy has dissipated. The case shown in Figure 7, four reflections are recorded.

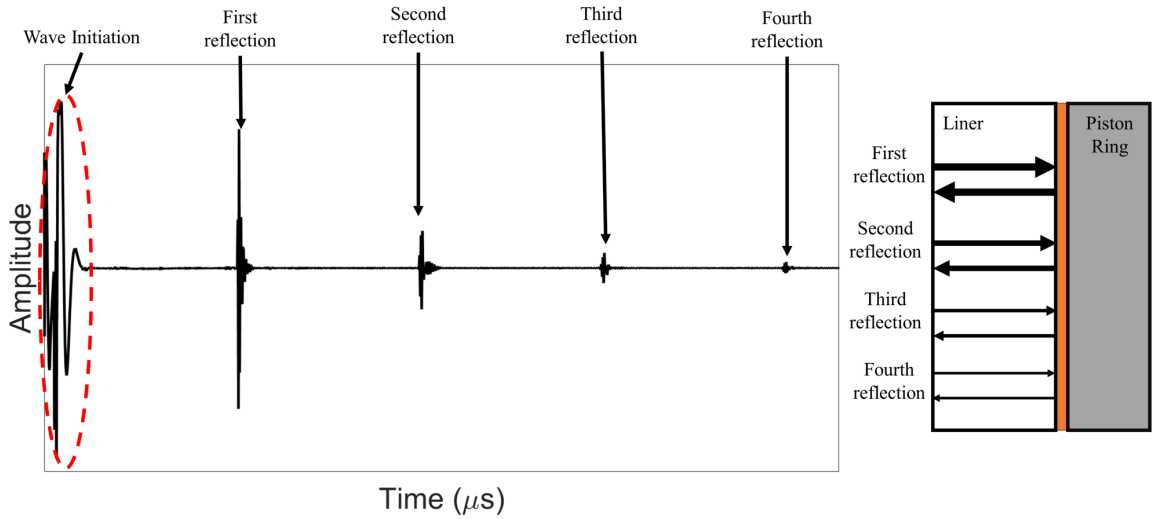

Figure 7 A typical A-Scan detailing four reflections from the internal surface of an engine liner. Note the four reflections occur at the same location yet the reflections are displayed down the liner for visualization purposes.

The ultrasonic pulses were controlled via an in-house LabVIEW program. Each data capture duration lasted for 5 seconds, this enabled multiple engine cycles to be covered during one capture and averaging of the oil film data. Through the course of the engine testing the ultrasonic pulse rate was varied; with some tests capturing A-Scans at 1.05 kHz per channel whilst other data captures focused on each transducer in turn at higher pulse rates of 12.4 kHz. At full engine load, single-channel measurements enabled A-Scans to be recorded up to a rate of one capture per 0.05 Crank Angle (CA). The recorded data was aligned to the engine crank angle using an encoder which produced a tick count from every TDC and every degree rotation of the crankshaft. A summary of the ultrasonic equipment used is shown in Figure 8.

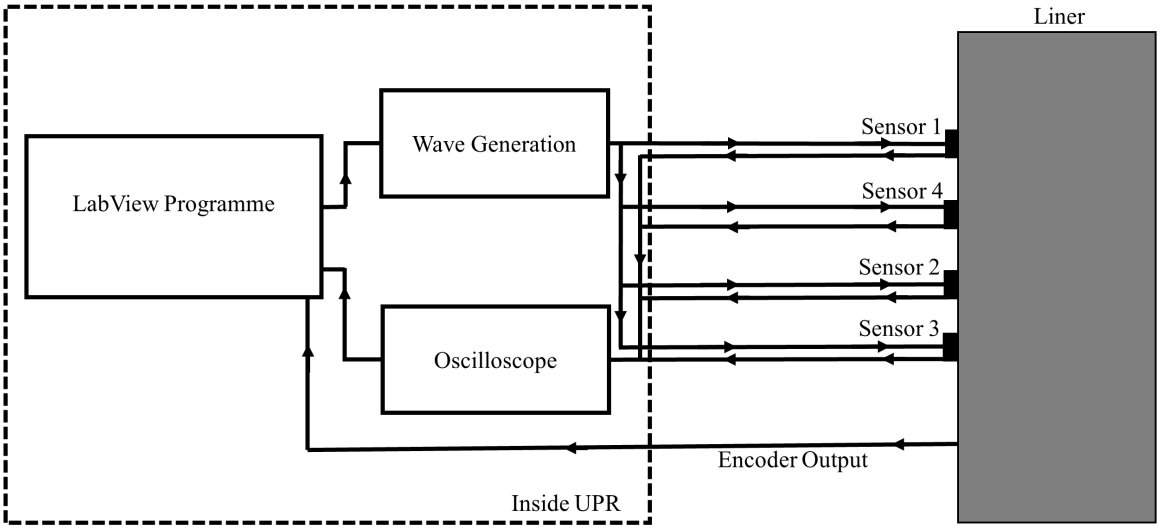

Figure 8 Ultrasonic testing equipment summary.

3.3 Test Conditions

The engine testing took place at three fired loading levels (100%, 50%, and 25%) each related to a different engine speed (105.5, 83.6, and 66.2 rpm respectively). Figure 9 (a) shows the engine loading sequence over a period of 8 hours (length of testing on each engine configuration).

Once the engine had achieved steady-state operation, the oil feed rate was varied from a nominal rate of 0.8 g/kWh to a low flow case of 0.6 g/kWh and then a high flow case of 1.2 g/kWh over the course of 20 minutes. This oil feed rate variation is summarised in Figure 9 (b) and was repeated at each engine load and for each of the three injector arrangements as previously shown in Table 2.

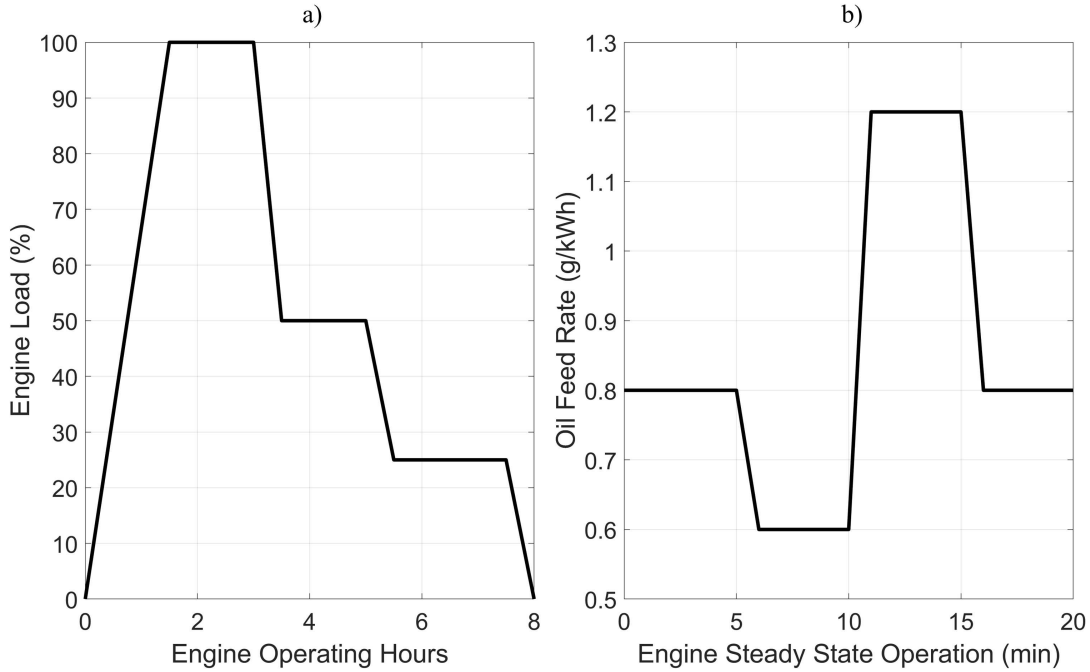

Figure 9 (a) Engine load variation over the course of testing for each engine configuration; (b) Oil feed rate variation across each steady-state operation period.

3.4 Signal Processing

The raw data was captured as a series of isolated A-Scan reflections see, Figure 10 (a) and (b). To convert this into oil film thickness measurements the preceding steps of Figure 10 were required.

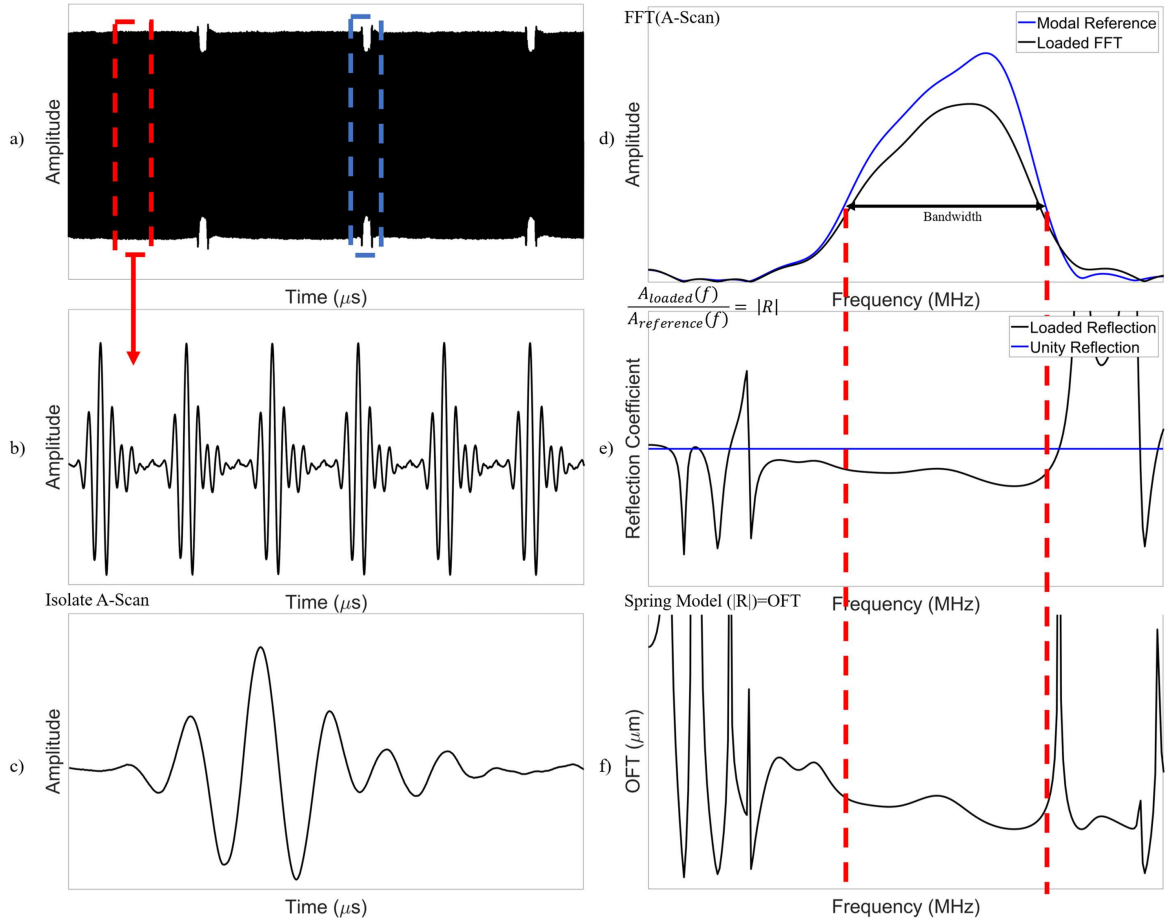

Figure 10 (a) Raw A-scan data, the highlighted blue region shows the change in A-scan amplitude that corresponds to a ring passing a transducer; (b) Zoomed in version of Figure 10 (a) showing the data consists of a series of A-scans. (c) Isolated individual A-Scan; (d) Modal FFT vs Loaded FFT; (e) Reflection coefficient variation over the frequency domain. The dashed line corresponds to R=1; (f) Oil film thickness over the frequency domain.

The ultrasonic reflection was isolated (Figure 10 (c)) and converted into the frequency domain using a fast Fourier transform (FFT) (Figure 10 (d)). Each FFT was normalized relative to the modal FFT to provide the reflection coefficient (Figure 10 (e)). The reflection coefficient was input into Equation 5, to output the oil film thickness (Figure 10 (f)). The oil film thickness calculation was refined by the application of Equations 6 and 7 from temperature and pressure measurements from the liner's internal surface.

The standard approach to provide a reference A-Scan is to obtain a measurement when the surface is unloaded and free from oil. As air is unable to support ultrasonic waves it leads to the greatest reflection amplitude achievable. In tests such as on the RTX-6 liner, this is unpractical therefore the reference measurements were taken whilst the piston was significantly far away from the transducers [25], see the red highlighted region in Figure 10 (a). This enables a modal reference to be calculated for each test that is subject to parameter variations during the testing, such as temperature variations and residual oil films on the liner surface [26]. Therefore, variations in the reflection coefficient are purely from piston movement over the measurement region of the transducers, see the blue highlighted region in Figure 10 (a). In some previous ultrasonic measurement works [32] the live reference measurement technique is applied with the addition of a correcting factor due to residual oil films that remains over the transducer outside of a loaded contact. This is typically applied in cases such as roller bearing studies as the raceways are often flooded with oil. This method has not been applied in this work due to the standard operation of piston rings being under starved lubricated conditions leading to minimal oil remaining on the internal surface of the liner.

4 Results

4.1 Reflection Coefficient

The technique outlined in the signal processing section has been applied to the A-Scans captured for the three injector configurations. In the case of Sensor 2, this experiences the first ring on its upstroke followed by the second ring at TDC and finally the first ring again on the downward stroke of the engine. These three stages are summarised in Figure 11.

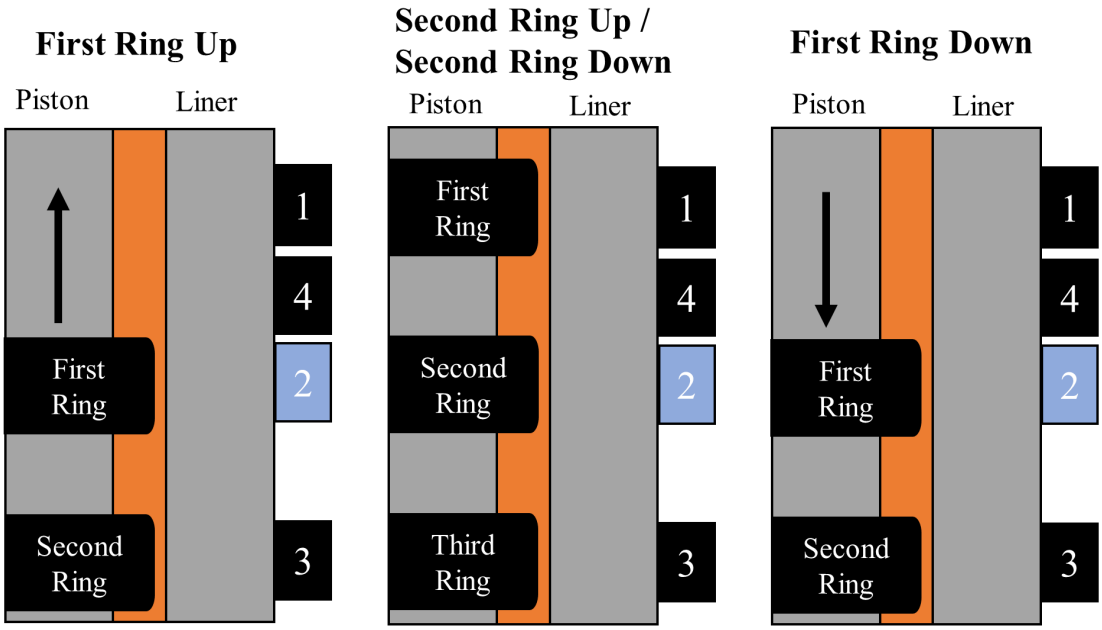

Figure 11 Ring passage over Sensor 2.

A labeled breakdown of the variation in reflection coefficient over Sensor 2 for a steady-state capture at 100% loading for all engine configurations is shown in Figure 12. Equivalent reflection coefficient variations are shown for Sensors 1, 3, and 4 in Figure 13-Figure 15 respectively. The crank angle measurement at the transducer location has been determined by calculation of piston ring displacement relative to its TDC location for the whole engine stroke. The crank angle corresponding to each piston ring moving over a transducer is highlighted in Figure 12-Figure 15 and is presented in terms of CA after TDC (aTDC) and was previously shown in Table 3. This breaks down complex variations in reflection coefficients into simpler trends.

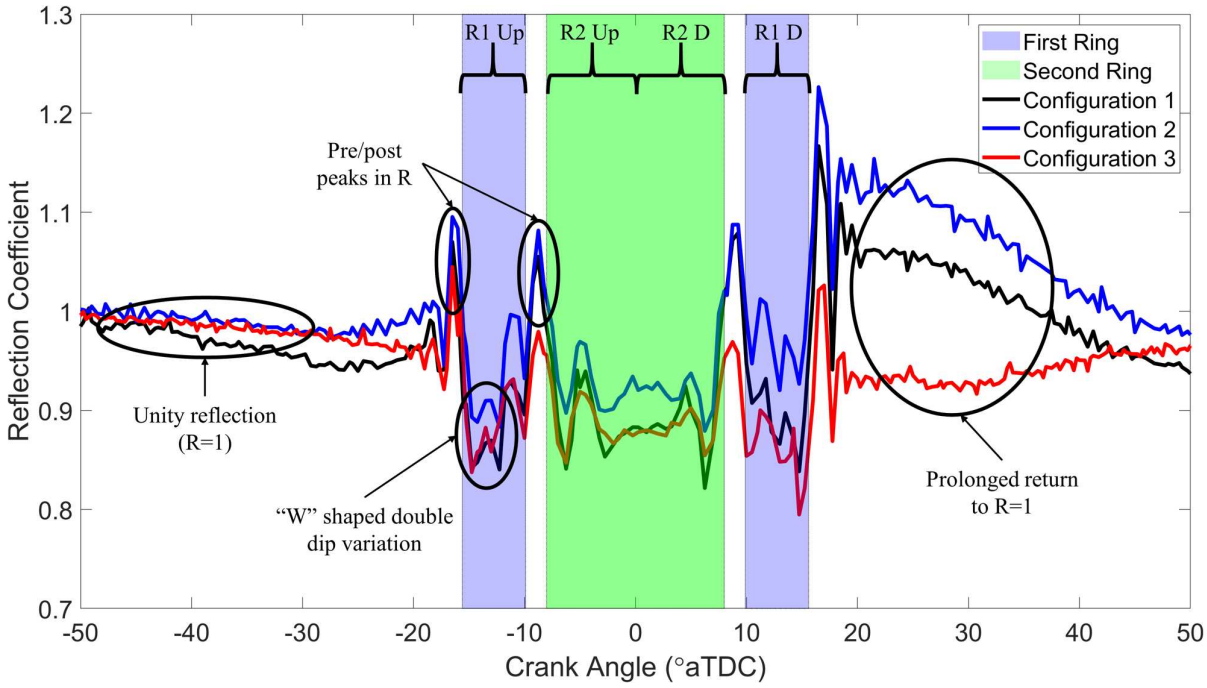

Figure 12 Reflection coefficient over Sensor 2, highlighting the two rings passing over the transducer.

Figure 12 covers Sensor 2 over a 100° CA range centered about TDC. On the piston approach to TDC the first ring passes at -15.6° to -9.9° CA, this corresponds to the R1 Up highlighted region in this figure. The reflection coefficient decreases from unity when the ultrasonic wave is partially transmitted through the oil film to the piston ring, with a greater reduction in *R* indicating greater transmission. Therefore, a lower value of *R* indicates a thinner lubricating film.

The green highlighted section signifies when the second ring is over Sensor 2, spanning from -8° to 8° CA, which is for the upward stroke of the second ring (R2 Up), the ring at TDC, and the preceding downward stroke of the ring (R2 D). As the piston is close to TDC in this region it is moving at a lower velocity leading to the second ring being positioned over Sensor 2 for a greater CA range. The ring is shown to be over this transducer at TDC as there is no increase in *R* at 0° CA.

The final region is the first ring moving over this transducer on the downward stroke (R1 D). The piston is at a greater velocity here leading to the ring moving over the transducer in a shorter CA range, leading to a narrower dip in *R*. With the increase in cylinder pressure typically leading to a greater reduction in *R* for this downward stroke than the upward stroke of the first ring (R1 Up).

In addition to major variations in reflection coefficient due to the rings moving over the sensing area of Sensor 2, there are other trends displayed in Figure 12. Outside of the measurement region of the piston rings the reflection coefficient largely remains around unity as this shows the complete reflection of the ultrasonic wave from the internal surface of the cylinder liner (i.e. no contact and no residual oil film). Whilst the reflection coefficients from when a piston ring is aligned with the transducer dips to 0.7 in some cases.

The general trend in reflection coefficient was the same for each engine configuration with the most prominent variations being from either; the magnitude of the dip, leading to changes in oil film thickness determined from the Spring Model or the variation in reflection coefficient after the last ring passed on the downward stroke for an extended crank angle range (> 20° CA). This may be an indication that an excessive oil film was left on the liner after the last ring passed, which dissipates as the reflection coefficient returns to unity.

For the regions of piston ring and sensor alignment, Configurations 1 and 3 provide near-identical reflection coefficient values whilst Configuration 2 is consistently higher. The upper rail injection system for Configuration 1 and 3 was the PJ injector vs NLT injector for Configuration 2. Displaying that the NLT injectors, with a reduced rate of lubricant atomization, led to a greater reflection of the ultrasonic signal and therefore thicker lubricating film.

Immediately before and after a piston ring moves over a transducer there is a sharp peak in the reflection coefficient above unity. The cause of which requires further study but there are a few potential causes; a leading/trailing oil wave, stress in the liner induced by the piston ring, the piston ring marginally outside of the measurement region causing a greater amount of ultrasonic energy to reflected towards to the sensor [33,34].

The micro variations within the dips in reflection coefficient are also noteworthy as in most cases there is a double-dip within each dip, leading to a "W" shape. The cause of this variation is unknown but may be due to several reasons; the movement of the piston ring traversing the piston ring groove, the piston ring itself tilting, or lateral movement of the ring towards and away from the liner on the neutral side [10]. For Sensor 2 this "W" shape is also more prominent in the upward stroke than downstroke, although this is not always the case, see Figure 14, Sensor 3. This pattern has been found in several other ultrasonic applications; piston skirt [24], roller bearing [33], and cold rolling [34]. These applications vary in geometry, lubricant presence, and speed of component displacement suggesting the cause of this is related to ultrasonic wave propagation instead of a geometric parameter of the engine.

The decrease in reflection coefficient is consistently greater for a ring on the downward stroke than the upward stroke, this is true for Sensor 2 (Figure 12) and the other sensors (Figure 13-Figure 15). This is likely due to the combustion process leading to an increased pressure in the cylinder thus causing the piston rings to conform more to the liner enabling greater transmission of the ultrasonic wave.

Similar variations are also seen for the other sensors, the same test cases as Sensor 2 in Figure 12 is shown for Sensors 1, 3, and 4 in Figure 13-Figure 15 respectively. Note the differing highlighted regions for the sensors as each sensor experiences piston rings moving over the sensing area at varying CA ranges as previously shown in Table 3.

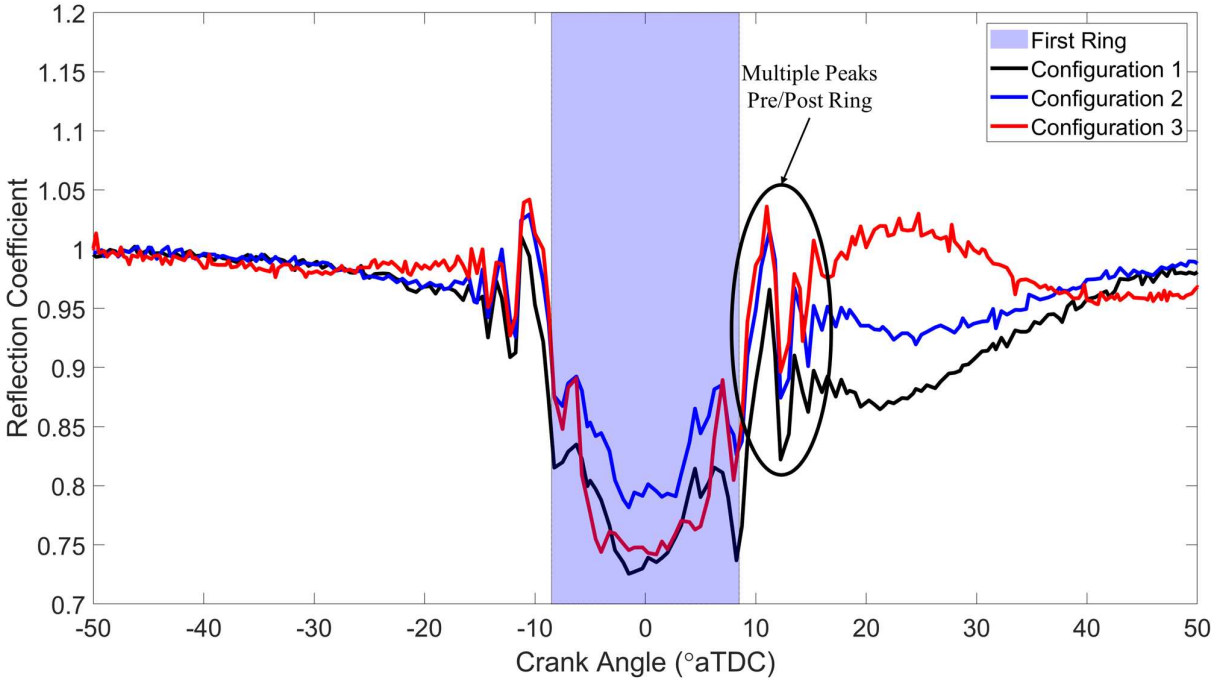

Figure 13 Reflection coefficient over Sensor 1, highlighting the first ring passing over the transducer.

The first ring is aligned with Sensor 1 at TDC, see Figure 13, this piston ring has a greater width than the other two piston rings and is therefore over the sensing area for a marginally greater range (-8.5° to 8.5° CA). In this plot, an additional trend is more pronounced, primarily as only one ring transverses this sensor. Further to the single peak in *R* pre/post ring observed in Figure 12, there is a series of cyclic peaks in *R*, highlighted in Figure 13. This pattern is more comparable to those seen in roller bearings [33] in which the cyclic peaks were shown to be independent of loading and occurring due to a roller approaching the sensing area leading to a greater amount of energy being directed back to the sensor.

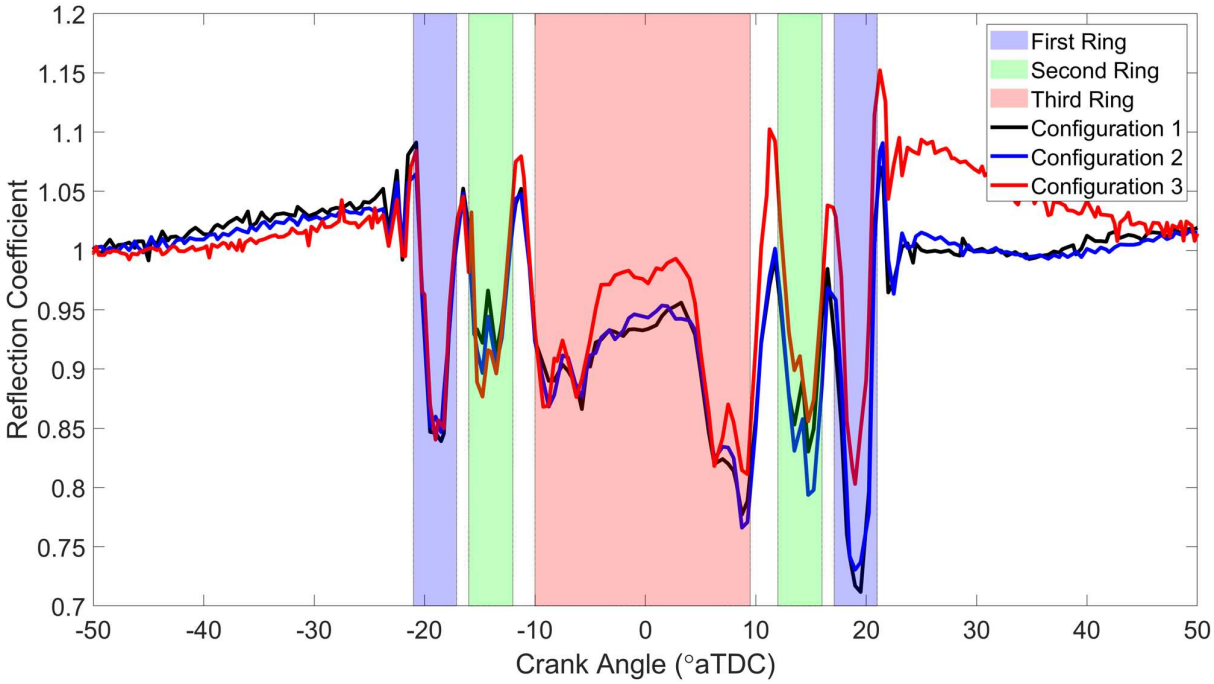

Figure 14 Reflection coefficient over Sensor 3, highlighting all three rings passing over the transducer.

The third sensor, Figure 14, has the most complex variation in reflection coefficient as all three piston rings move past this sensor with the third ring aligned with it at TDC. The first ring moves over this sensor at -21° to -17.1° CA followed by the second ring at -16° to -11° CA. The two have largely similar trends in reflection coefficient over a comparable sized CA range although the second ring experiences the "W" shape highlighted for Figure 12 yet the first ring does not. The third sensor was aligned with the third ring over a large range (-9.2° to 9.2° CA) covering TDC. Although the reflection coefficient returns to near unity over -5° to 5° CA. This may indicate the transducer was positioned marginally too far down the liner and is beneath the third ring at TDC.

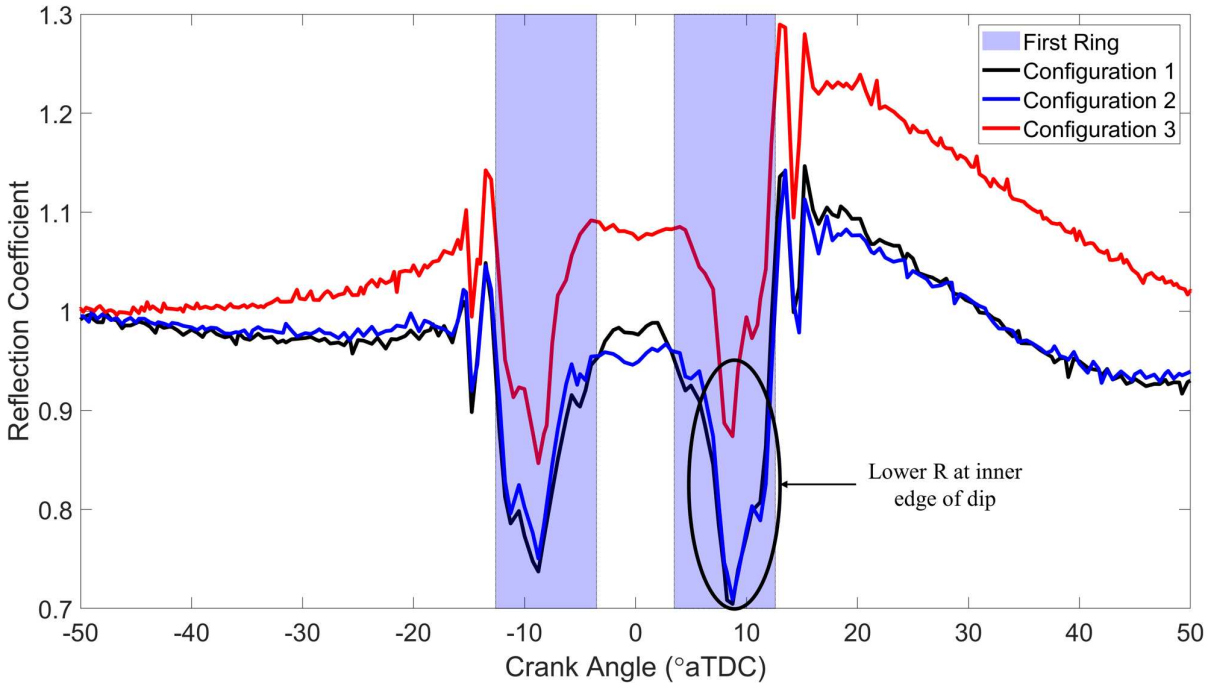

Figure 15 Reflection coefficient over Sensor 4, highlighting the first ring passing over the transducer.

Sensor 4, seen in Figure 15, is positioned between the first and second ring at TDC. This leads to the first ring moving past this transducer shortly before and after TDC, hence two dips in reflection coefficient. This sensor displays a deviation on the "W" dip variation experienced by other transducers, with the inner edge (edge closer to TDC) having a lower reflection coefficient. This may indicate the ring is tilted with the lower section of the piston ring closer to the liner.

4.2 Effect of Pulsing Rate

Through the course of this work, there were two different methods to record A-Scans, recording all channels (sensors) at once at a lower pulse rate of 1.05 kHz, or focusing on a single channel in turn to allow a higher pulse rate of 12.4 kHz. Figure 16 shows the variation in reflection coefficient for Sensors 1-4 for the two different pulse rates used at 50% engine loading.

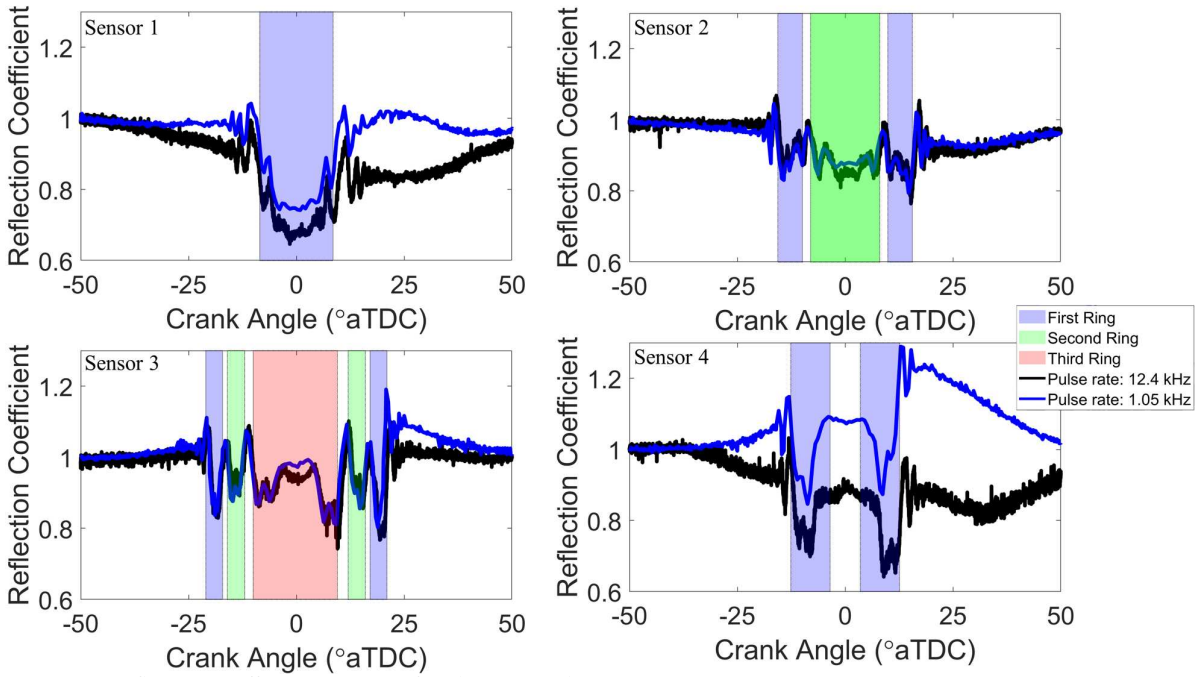

Figure 16 Reflection coefficient variation for changing pulse rate.

A pulse rate of 1.05 kHz leads to an A-scan capture every 0.6° CA whereas using 12.4 kHz provides a measurement every 0.05° CA but limits the data to be recorded on each channel in turn. The effect of increasing the pulse rate on the reflection coefficient is only clear for Sensors 1 and 4 which provides a significant reduction in the reflection coefficient. Figure 15, Sensor 4, previously displayed a lower reflection coefficient at the inner edge of the ring implying ring tilt. However, the increased pulse rate has removed this trend for Sensor 4 and now provides a "W" shape such as seen for the other sensors. Observation of plots (b) and (c) for Sensors 2 and 3 show minor differences between the two pulse rates with the most prominent change arising close to TDC with the increased pulse rate leading to a lower reflection coefficient value. Note, the single-channel measurements were taken over a short period of 50% loading marginally outside of the steady-state testing period whilst the slower pulse rate was within the steady-state operation period.

5.3 Spectrograms

Observation of the reflection coefficient over the whole bandwidth of the transducers provides a more complete view of the variation in reflection coefficient over an engine cycle. This is shown in Figure 17 (a)-(c) for Sensor 1 for the three engine configurations at 100% loading. In these plots, 1 MHz has been highlighted with a dashed line as this is the frequency used previously in Figure 12-Figure 16, in addition to being used for oil film thickness calculations in the following section. The spectrograms have been limited to the range of $0.9 < R < 1.1$, this has been done for visualization purposes to center the reflection coefficient around unity (R=1) and to display the trends in the reflection coefficient clearer.

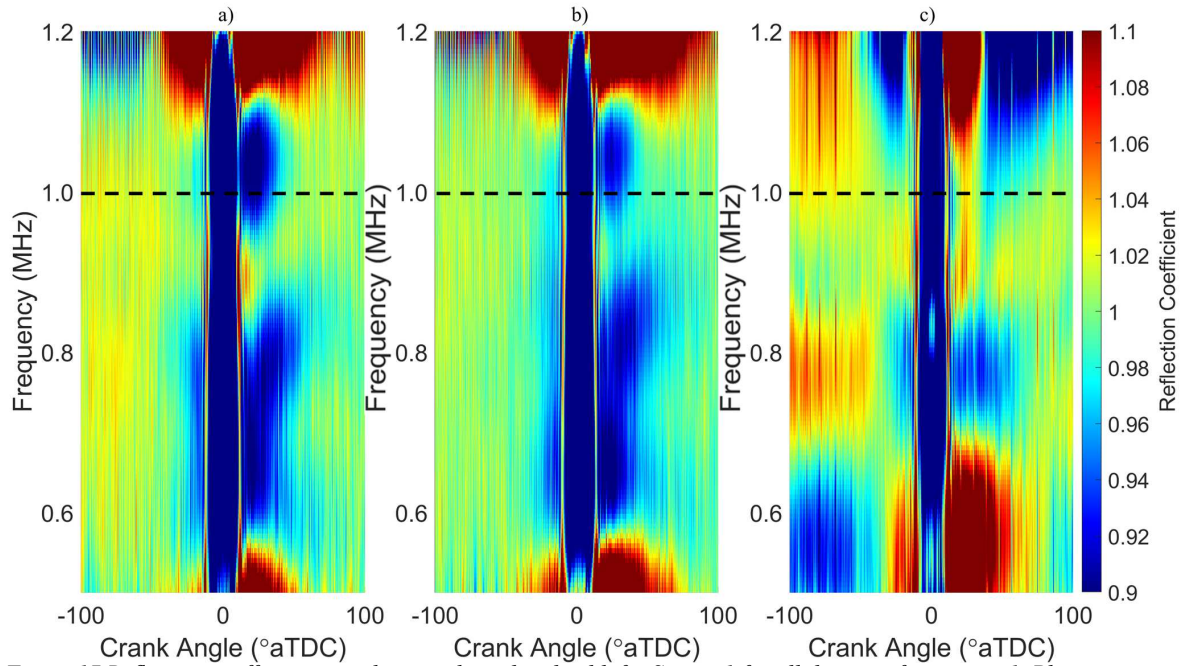

Figure 17 Reflection coefficient over the transducer bandwidth for Sensor 1 for all three configurations 1. Plots a-c correspond to Configurations 1-3 respectively. 1 MHz is highlighted as this frequency was used for oil film thickness calculation.

The spectrograms for the three engine configurations over the bandwidth of Sensor 1, Figure 17, largely show a consistent decrease in reflection coefficient beyond 0.9 *R* across the whole bandwidth for -8.5° to 8.5° CA which corresponds to when the first ring is aligned with this transducer.

Outside of the region corresponding to the first ring, there are bands of increased and decreased reflection coefficient which vary with frequency across the bandwidth of the transducer. Along the 1 MHz line the band of increased/decreased reflection coefficient post ring is the same as the "Prolonged return to *R*=1" section seen in Figure 13. The cause of these frequency-dependent bands of reflection coefficient variation is unknown but may be an indication of the residual oil film left on the liner post ring.

Observation of Figure 17 (a) and (b) which resembles Configurations 1 and 2 shows a near-identical variation in reflection coefficient across the whole bandwidth. Yet the third configuration displays significantly different patterns outside of the first ring zone. This may be an indication of transducer deterioration over time or a largely differing residual oil film left from the third configuration which is unexpected due to the upper rail for Configuration 1 and 3 being the same.

For the preceding work, a frequency index of 1 MHz was used, this was primarily due to the center frequency of these transducers being 1 MHz, although it is clear from Figure 17 that the selection of this frequency index has an effect on the resulting reflection coefficient and thus oil film thickness.

4.4 Oil Film Thickness

The reflection coefficient of Figure 12-Figure 15 has been used to determine the oil film thickness (OFT) between the piston ring and cylinder liner using Equation 5. The same 100% loading test cases as shown in Figure 12 are shown in Figure 18 which refers to Sensor 2. Whilst Figure 19-Figure 21 show Sensors 1, 3, and 4 respectively.

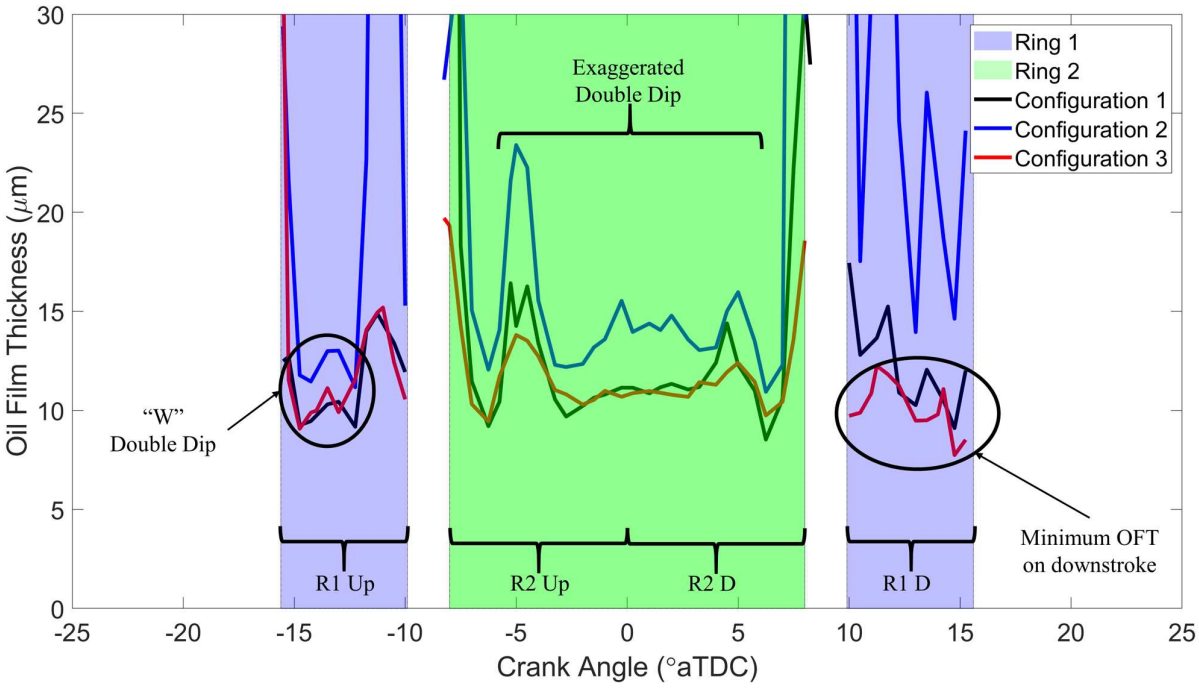

Figure 18 Oil film thickness measurements over Sensor 2 for 100% engine loading steady-state operation.

The oil film thickness shown in Figure 18, for Sensor 2, is of the same order of magnitude for each engine configuration. The upper rail in the second configuration was the NLT injector (the injector design that reduced atomization of the lubricant) reducing lubricant presence in the exhaust manifold. This is directly reflected in the OFT, with Configuration 2 providing thicker lubricating films, roughly 4 μm thicker at TDC than the other configurations. Whilst Configurations 1 and 3, both with PJ injectors on the upper rail provided near identical film thicknesses.

The "W" shaped double-dip present in the R1 Up reflection coefficient of Sensor 2 (Figure 12) remains present in the OFT over this sensor. Whilst the second ring (R2 Up and R2 D) now displayed an exaggerated version of the double-dip, with a "W" at either side of the ring passage. No double-dip is displayed for R1 D, instead, the OFT decreases over the passage of the ring with minimum oil film thickness at 14.5° CA, once the ring has almost moved completely past the transducer. This is shortly after the maximum combustion pressure and therefore may be due to the cylinder pressure causing the ring to conform more to the liner, potentially with the addition of ring tilt or ring lateral movement.

The OFT greatly increases either side of all the rings, Takiguchi [13] and Seki et al. [14] argued this is likely a bow wave pre-and post- ring passage. Yet works such as Garcia-Atance Fatijo et al. [10] who used capacitance transducers, showed the rings operated under starved conditions and indicated potential flow detachment therefore it is not necessarily a bow wave of lubricant.

The same general trends in oil film thickness are observed for Sensors 1, 3, and 4 as shown in Figure 19-Figure 21 respectively. Note the differing highlighted regions for each sensor as each experienced piston rings moving over the sensing area at varying CA ranges.

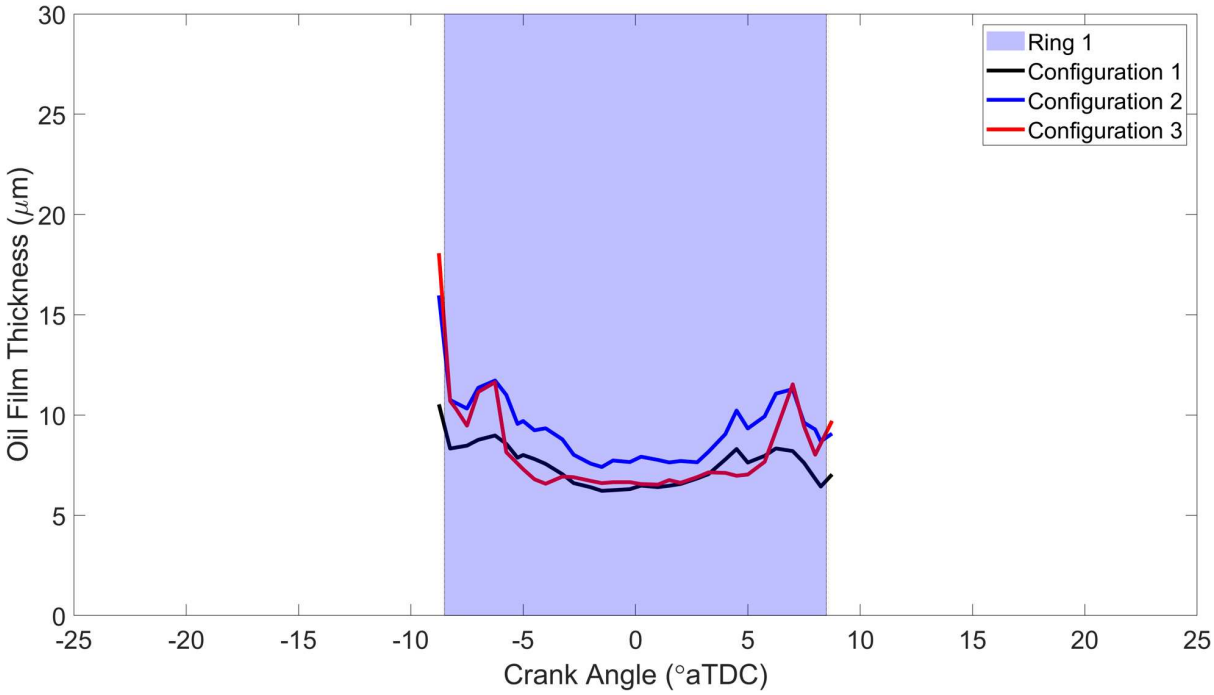

Figure 19 Oil film thickness measurements over Sensor 1 for 100% engine loading steady-state operation.

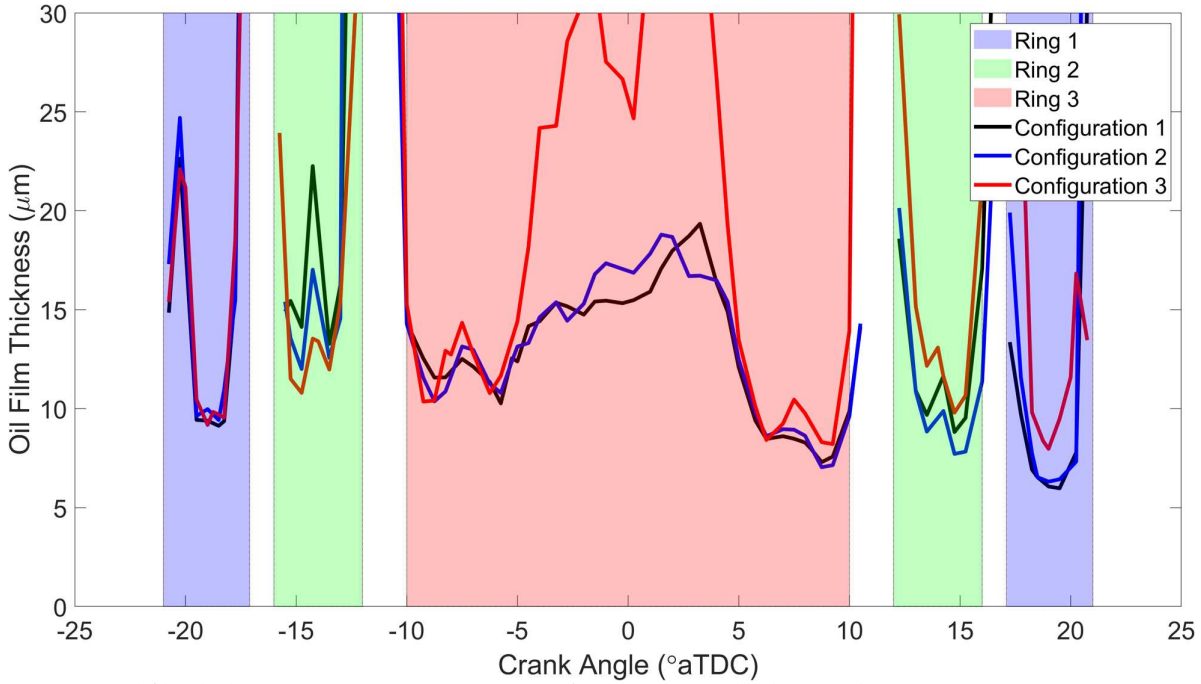

Figure 20 Oil film thickness measurements over Sensor 3 for 100% engine loading steady-state operation.

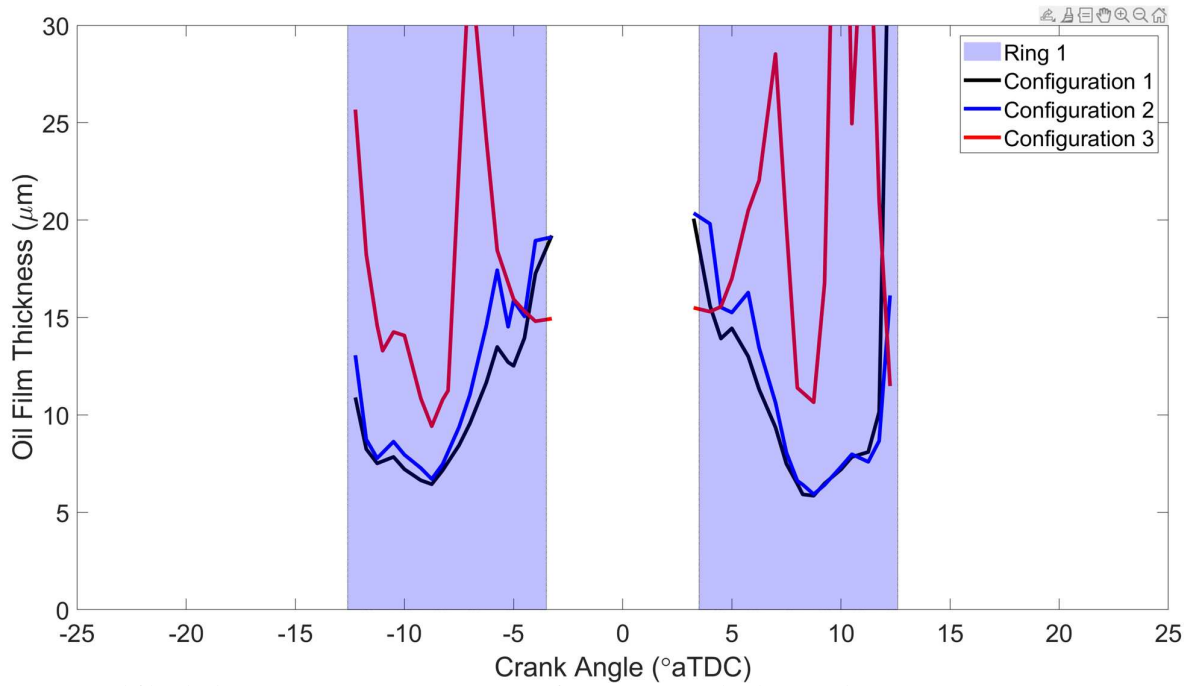

Figure 21 Oil film thickness measurements over Sensor 4 for 100% engine loading steady-state operation.

Similar trends are shown for the three engine configurations for all piston rings in Figure 18-Figure 21, except for the third configuration in Sensor 3 Ring 3 (Figure 20) and Sensor 4 Ring 1 (Figure 21) which shows significantly differing patterns. This is thought to have been due to either the sensors having moved or malfunctioned after extended use as Configuration 3 was the last to be tested.

The oil film thickness is shown in Figure 18-Figure 21 shows the rings further up the liner (Sensors 1 and 4) to have minimum OFT values of significantly less than 10 µm, typically around 7 µm whereas sensors further down the liner (Sensors 2 and 3) have minimum OFT values around 10 µm. This is likely the case as the first ring can be seen as a buffer ring between high and low pressure regions and this ring moves over Sensors 1 and 4 closer to TDC when the combustion chamber experiences greater pressures. The high pressure of the combustion chamber causes the ring to conform to the liner more leading to a thinner oil film between the two. The combustion pressure also affects Sensors 1, 3, and 4 as previously mentioned for Sensor 2 (Figure 18) causing the downstrokes for each ring to be thinner than their respective upward strokes.

Comparable to Sensor 2 (Figure 18) double dips in the OFT are displayed for Sensor 3 (Figure 20) although they are not prevalent for the first ring moving over this transducer for either the up or the downstroke. This piston ring moved over the sensing area of Sensor 3 at a greater velocity, therefore there were fewer A-Scans captured in this timeframe, potentially leading to there not be enough data points to show the double-dip. Whilst Sensor 4 (Figure 21), like its reflection coefficient shows the inner edge OFT to be the thinnest point.

Sensors 1-3 are aligned with the first, second, and third piston ring respectively at TDC. At this location in Figure 18-Figure 20, Configuration 2 consistently provides a thicker lubricant film than the other two configurations, excluding Configuration 3 for Sensor 3 as the sensor is thought to have moved or malfunctioned here.

4.5 Minimum Oil Film Thickness Variation with Speed/Load

The minimum oil film thickness (MOFT) for each data capture has been calculated by application of the Spring Model to each engine cycle. Comparison of the MOFT for the three engine configurations for the first piston ring at TDC is shown in Figure 22 with the corresponding engine speed for that capture.

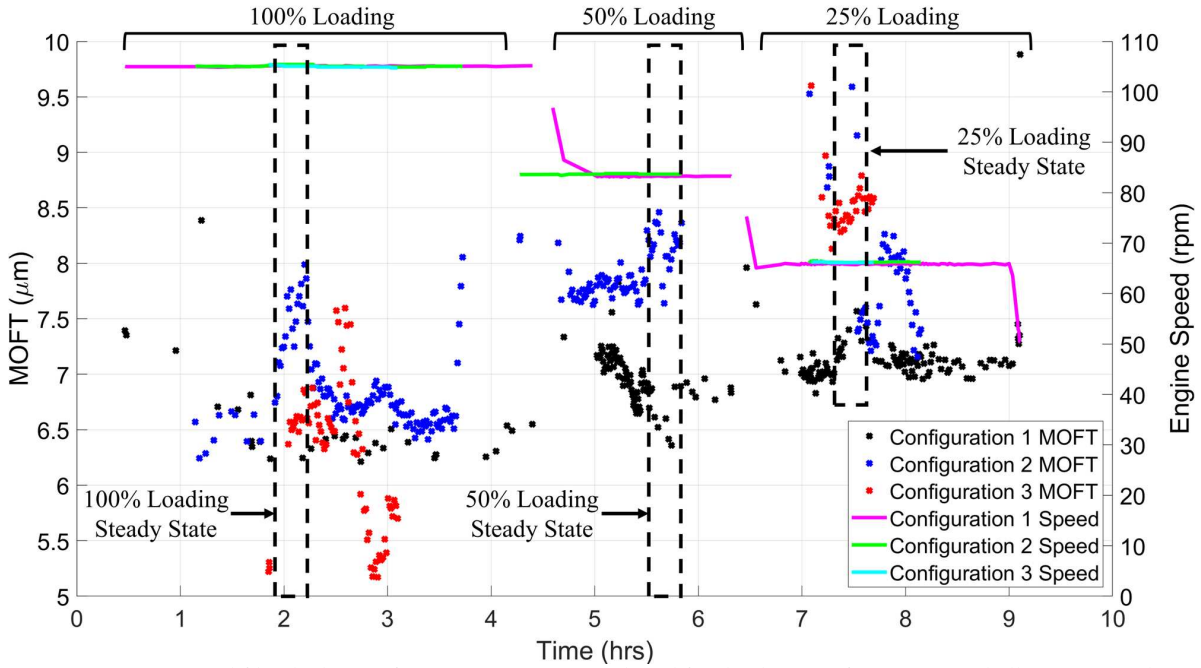

Figure 22 Minimum oil film thickness of Ring 1 over Sensor 1 plotted for the three configurations and all engine speed levels. The three steady-state operation periods are highlighted via dashed boxes.

Across all three engine configurations, the trend of increased lubricant film thickness with decreased engine load is observed. For example, Configuration 1 steady-state MOFT values are 6.3 µm, 6.7 µm, and 7.3 µm for 100%, 50%, and 25% loading respectively. There are several contributing factors to this trend, at higher engine loading, the combustion pressure is greater, leading to greater ring conformity to the liner. In addition to this, the higher internal liner temperature and pressure results in a lower oil speed of sound and oil density, reducing the lubricant film thickness. The increased liner temperature also causes an increased rate of lubricant evaporation therefore there is less lubricant present to form an oil film at higher engine loads. The lubricant flash temperature is 220 ℃ and at 100% engine loading the liner's internal surface temperature is 216 ℃ at the location of Sensor 1. The ring surface temperature is likely higher than this leading to a greater rate of oil evaporation. All of these factors compound to results in a thinner lubricant film at higher engine loading.

Figure 22 shows that the MOFT of the first ring over Sensor 1 is greater for Configuration 2 than Configurations 1 and 3, during steady-state operation, except at the end of the 25% loading period. A greater MOFT consequently reduces the likelihood of boundary lubrication (metal-metal contact) occurring between the piston ring and cylinder liner. For steady-state testing at 100% and 50% loading, Configuration 2 provided a film that was consistently at least 17.5% thicker than the two other engine configurations. This configuration was the lubricating system with a reduced rate of lubricant atomization, ultimately reducing lubricant losses to the exhaust manifold. This led to a greater amount of injected oil remaining within the cylinder which was directly reflected in terms of a greater MOFT for Configuration 2.

Outside of steady-state operation, outside the dashed boxes in Figure 22, the MOFT for Configuration 2 is greater than that of the other two configurations at all points except a short period of Configuration 3-100% loading where the MOFT increased. In general, the MOFT is relatively consistent outside of steady-state loading except brief instances for Configuration 3-100% and Configuration 2-25% the cause of which is unknown.

4.6 Effect of Change in Oil Feed Rate

The RTX-6 engine experienced a 20-minute steady-state operation period for each engine loading with each injector configuration. Within these steady-state periods the oil feed rate (OFR) was varied

as shown previously in Figure 9 (b). The MOFT values measured during this period are shown in Figure 23 for the first ring moving over the four sensors in CA order, with the change in OFR plotted in green. For example, the order the first ring passes the sensors is 3, 2, 4, 1 (TDC), 4, 2, 3, hence left to right for upstrokes followed by right to left for downstrokes. The equivalent plots for the second and third rings moving over their respective transducers are shown in Figure 24 (a)-(c).

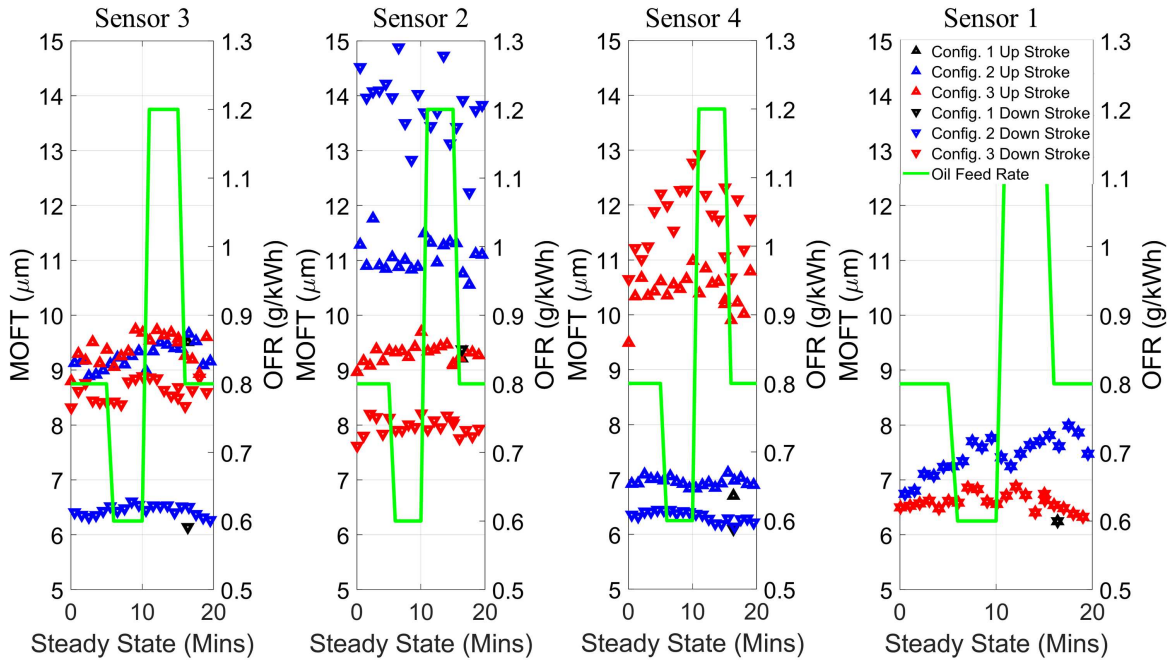

Figure 23 MOFT of the first ring over Sensors 1-4 for up and down strokes for all configurations at 100% loading with the addition of oil feed rate change.

All four plots in Figure 23 display no clear variation in MOFT with the change in OFR for the first piston ring, this was also demonstrated for the 50% and 25% loading. It is not clear why there is no definitive variation in MOFT with OFR. Possibly film formation is simply not sensitive to the amount of oil present, provided a certain threshold volume is supplied; and testing was all carried out above that threshold. Additionally, the OFR steps were in intervals of 5 minutes which may not have been a significant enough time to lead to a change in the lubricating film thickness.

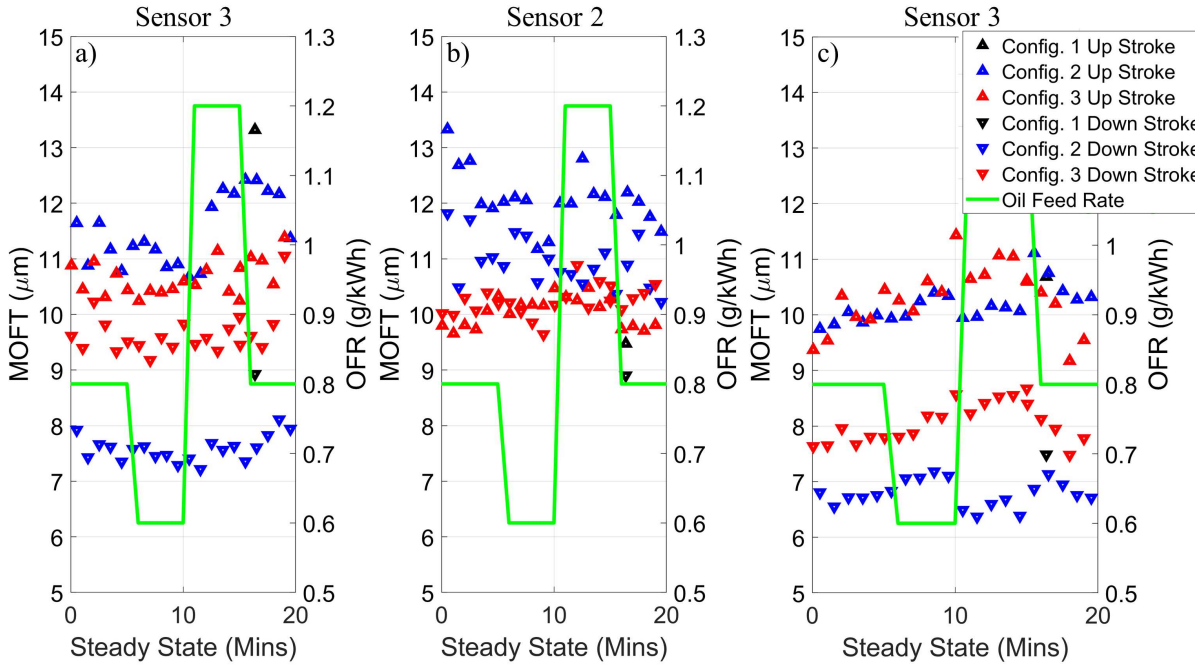

Figure 24 MOFT of the second and third ring over Sensors 2-3 for up and down strokes for all configurations at 100% loading with the addition of oil feed rate change; plots (a) and (b) refer to Ring 2 whilst plot (c) refers to Ring 3.

Figure 24 (a) and (b) show the change in MOFT with OFR for the second ring moving over Sensors 3 and 2, respectively. Whilst Figure 24 (c) is for the third ring over Sensor 3. Similar to the results for the first ring (Figure 23) there is no clear change in MOFT with OFR for either of the other two piston rings.

4.7 Measurement Repeatability

The previous section displays the MOFT across the steady-state period for 100% engine loading. The change in MOFT over this interval is explored in greater detail for all engine loading levels in Figure 25-Figure 27. These figures show the mean MOFT over this period for each engine configuration and loading with the addition of the standard deviation.

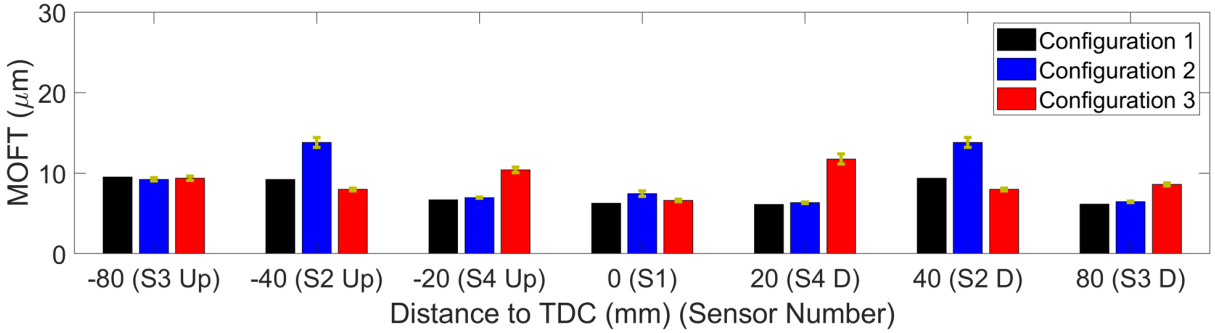

Figure 25 MOFT of 100% engine loading for the first ring moving across the sensors with the standard deviation of MOFT. Note, there are no standard deviations for Configuration 1 as there was only one measurement taken within this steady-state period.

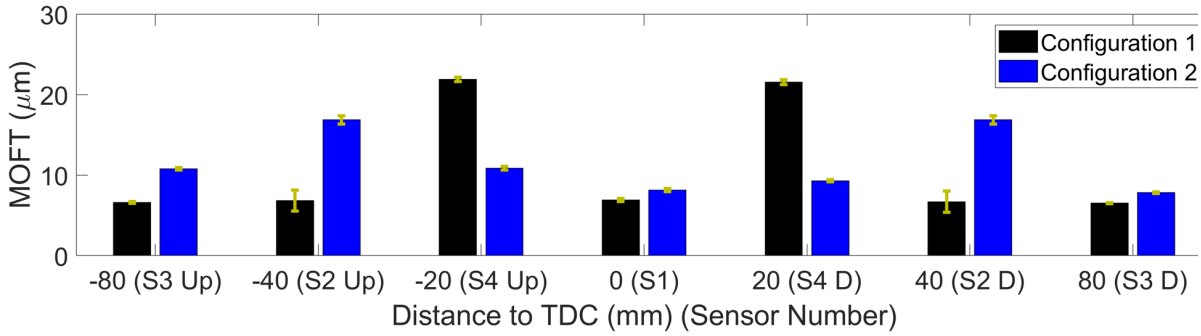

Figure 26 MOFT of 50% engine loading for the first ring moving across the sensors with the standard deviation of MOFT.

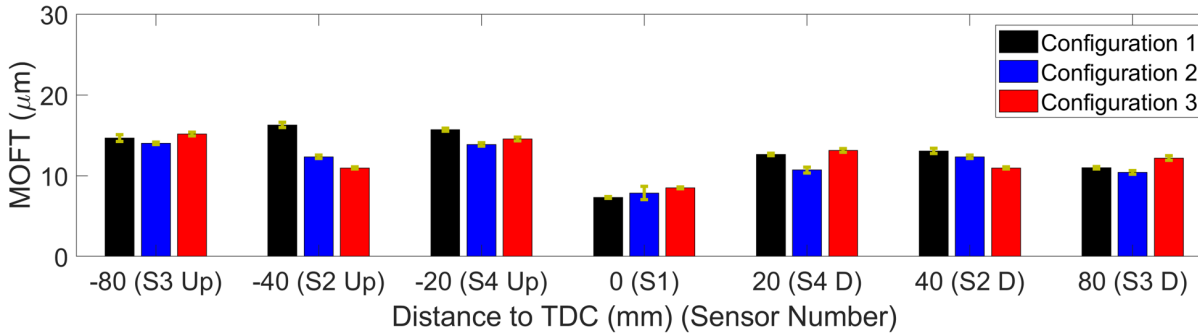

Figure 27 MOFT of 25% engine loading for the first ring moving across the sensors with the standard deviation of MOFT.

Across all engine configurations and loading levels in Figure 25-Figure 27, the first piston ring has the thinnest oil film when the ring is at TDC, with Configuration 1 providing a thinner film than the other two configurations. The standard deviation of MOFT across the steady-state period varies from ±0.07 µm up to ±1.3 µm with the least variation consistently occurring at TDC.

Sensor 2 often provided a thicker MOFT than the sensors on either side. With this sensor having the greatest standard deviation in results (±1.3 µm), it can be seen in Figure 23 and Figure 24 that this increased variation in results is no indication of a greater variety of MOFT with OFR. This sensor may be providing thicker MOFT measurements with a greater variation due to a potential transducer issue such as a marginal error in transducer placement leading to a coolant channel being partially over the measurement area or insufficient bonding between the sensor and external liner surface. Excluding Sensor 2, the maximum standard deviation over steady-state operation is ±0.9 µm across all rings traversing all sensors, further indicating there is no definitive change in MOFT with OFR.

The MOFT is numerically shown in Table 4-Table 6 for the first piston ring moving across all sensors for the three engine configurations and loading levels. These tables include the addition of the coefficient of variance (COV) over the steady-state period.

Table 4 Steady-state MOFT across 100% loading for all configurations for the first piston ring passing all transducers. Note, there are no coefficients of variance values for Configuration 1 as there was only one measurement taken within this steady-state period.

Configuration	**Dist to TDC (mm) Sensor Up/Down Stroke**	**-80 S3 UP**	**-40 S2 UP**	**-20 S4 UP**	**0 S1**	**20 S4 D**	**40 S2 D**	**80 S3 D**
1	MOFT (µm)	9.5	9.2	6.7	6.3	6.1	9.4	6.1
	COV (%)	-	-	-	-	-	-	-
2	MOFT (µm)	9.2	11.1	7.0	7.4	6.3	13.8	6.5
	COV (%)	2.3	2.6	1.2	4.6	1.5	4.5	1.4
3	MOFT (µm)	9.4	9.3	10.4	6.6	11.8	8.0	8.6

	COV (%)	2.9	2.0	3.3	2.3	5.4	2.0	2.3

Table 5 Steady-state MOFT across 50% loading for all configurations for the first piston ring passing all transducers.

Configuration	Dist to TDC (mm) Sensor Up/Down Stroke	-80 S3 UP	-40 S2 UP	-20 S4 UP	0 S1	20 S4 D	40 S2 D	80 S3 D
1	MOFT (µm)	10.2	22.9	11.0	6.7	10.8	18.8	7.7
	COV (%)	1.2	6.5	2.5	3.0	2.9	7.0	0.9
2	MOFT (µm)	10.8	21.2	10.9	8.1	9.3	16.9	7.8
	COV (%)	1.4	3.1	2.1	2.4	1.6	3.1	1.2

Table 6 Steady-state MOFT across 25% loading for all configurations for the first piston ring passing all transducers.

Configuration	Dist to TDC (mm) Sensor Up/Down Stroke	-80 S3 UP	-40 S2 UP	-20 S4 UP	0 S1	20 S4 D	40 S2 D	80 S3 D
1	MOFT (µm)	14.7	16.3	15.7	7.3	12.6	13.1	11.0
	COV (%)	2.9	2.2	1.3	1.8	1.3	2.4	1.4
2	MOFT (µm)	14.0	14.7	13.9	7.9	10.7	12.3	10.4
	COV (%)	1.1	1.7	1.5	10.4	3.5	1.7	2.1
3	MOFT (µm)	15.2	15.8	14.5	8.5	13.1	11.0	12.2
	COV (%)	1.5	1.2	1.5	1.5	1.9	1.2	2.5

5 Discussion

Ultrasonic reflectometry has been applied to a fired two-stroke RTX-6 engine to quantify the oil film thickness for three piston rings moving across four piezoelectric transducers. With MOFT values for the first piston ring ranging from 6-22 µm. To provide these values several assumptions have been made and limitations identified which are discussed in the following section. In addition the MOFT from the RTX-6 is compared to oil film thickness measurements from alternative engines in this section.

5.1 Assumptions and Limitations

The temperature used to define the oil speed of sound and density was determined from temperature measurements from the internal surface of the liner. It was assumed that the temperature of the oil in the contact was the same as this surface temperature. The flash temperature of the ring will have likely been significantly higher and vary with engine CA especially during the early stages of the power stroke. For 100% loading, all piston rings were assumed to be at 216 °C, however, an increase of 10 °C reduces the oil film thickness calculated by 0.3 µm. This factor will have affected all measurements equally, therefore the trends in results remain unchanged.

The ultrasonic transducers have provided OFT measurements that are similar to previous works with some of the same trends identified from alternative techniques, highlighting their robustness. Yet potential issues with either bonding, placement or damage, may have led to different trends in reflection coefficient to be seen in the third testing configuration. Sensor 2 for example provides consistently higher film thickness measurements than transducers on either side indicating that the transducer may have been positioned incorrectly.

The spatial resolution of the sensors in this work was notably improved from previous ultrasonic ring-liner measurements [5, 23-28]. With most of the previous research using piezoelectric transducers equal to or greater than the size of the first piston ring yet this work used transducers smaller than any

of the rings (14 mm active element diameter). Therefore, the averaging effect from the ultrasonic transducers was minimized when the sensing area was completely encompassed by a piston ring, aided further by the barrelled profile of the rings with the edges having small radii curvatures. However, the spring model applied in this work is only applicable for a solid-oil-solid system, therefore it is only applicable when the piston ring is over the sensor. When the piston ring is marginally over the contact there is a combination of a partial solid-oil-solid system and a solid-oil system which inhibits the applicability of the spring model. The averaging effect of the ultrasonic transducers will have led to an overestimation of the lubricant film thickness in this region due to higher reflection coefficients being measured than caused purely from the piston ring itself.

It has been assumed that any changes in the reflection coefficient were purely from a piston ring moving over a transducer. For this to be the case the region between the piston ring and liner must be fully flooded with lubricating oil. Yet piston rings often operate under starved conditions or cavitation may occur in the lubricating film. Either of these factors would have led to a higher reflection coefficient than if the region were fully flooded with oil. Therefore, the OFT presented here is likely an overestimation of the true OFT especially for OFT values significantly far from the MOFT.

5.2 Comparison to Other works

The oil film thickness between a piston ring and cylinder liner has been the focus of numerous works, as highlighted in the opening section of this paper, with most of that research focusing on smaller engines. Due to this, their comparison to a large diesel marine engine is somewhat limited. The MOFT from previous research typically varies from 0.2-20 μm across all techniques [5-29] with ultrasound providing measurements from 2-20 μm [5, 23-29]. The OFT from the RTX-6 is thinnest for the first ring at TDC (6.3 μm Configuration 1), which is close to the MOFT from a Winterthur Gas & Diesel RTX-4 engine of 6 μm [29]. These values are a factor of 3 larger than their automotive counterparts which may partially be from a larger engine operating at much greater loads and partially from this work being on the neutral side of the engine as most previous works study the thrust or anti thrust side.

6 Conclusion

The lubricating film between a piston ring and cylinder liner in a large diesel marine engine has been quantified using ultrasonic reflectometry by positioning piezoelectric transducers close to top dead center on the outer surface of an RTX-6. This oil film is a key contributor to engine emissions with lubricant thrown off into the combustion chamber raising particulate emissions and wasting oil. However, if the lubricating film is too thin it leads to metal-metal contact and damage to engine components.

The thickness of this lubricating film has been quantified for three engine loading levels across three different cylinder lubricant injection configurations each with varying rates of lubricant atomization. Across all three injection systems, the oil film thickness increased with decreased engine loading. Configuration 2 provided a thicker minimum oil film thickness for the first ring at top dead center than either of the other two engine configurations. Configuration 2 minimum oil film thickness was 7.4 μm instead of 6.3 μm and 6.6 μm for Configurations 1 and 3 respectively. Engine Configuration 2 used needle lift type injectors on the upper rail which reduced the rate of lubricant atomization reducing lubricant losses to the exhaust manifold whilst it also increased the thickness of the lubricating film. It is, therefore, reasonable to conclude that this engine configuration reduces engine emissions, by a smaller loss of lubricant whilst also improving the lubrication regime of the piston rings close to top dead center avoiding boundary lubrication.

Within each loading and engine configuration, the oil feed rate was varied from its nominal rate to an upper and lower rate in 5-minute intervals. Measurements of the minimum oil film thickness during

this time display no clear trend between minimum oil film thickness and oil feed rate. This is expected to be the case due to the short intervals of the change in oil feed rate.

References

[1] International Maritime Organization, “Resolution MEPC.304(72) – Initial IMO strategy on reduction of GHG emissions from ships” International Maritime Organization, April 2018. Accessed July 11, 2020. Available at: https://www.imo.org/en/OurWork/Environment/Pages/Technical-Co-operation.aspx.

[2] Tung, S., and McMillian, M., “Automotive tribology overview of current advances and challenges for the future,” *Tribology International* 37, no. 7 (2004): 517-536, doi:10.1016/j.triboint.2004.01.013.

[3] Froelund, K., Fritz, S. and Smith, B. “Lubricating oil consumption measurements on an EMD 16-645 Locomotive Diesel Engine,” Paper presented at Spring Technical Conference or the ASME Internal Combustion Engine Division, Salzburg, Austria, May 11-14 2003.

[4] Froelund, K., and Yilmaz, E. “Impact of engine oil consumption on particulate emissions,” Paper presented at International Conference on Autmotive Technology, Istanbul, Turkey, November 26 2004.

[5] Mills, R., Avan, E., and Dwyer-Joyce, R., “Measuring Lubricating Films at the Piston-Cylinder Contact: An Overview of Current Technologies with Focus on Ultrasound,” SAE Technical Paper 2013-01-0294, 2013 doi:10.4271/2013-01-0294.

[6] Takiguchi, M., Sasaki, R. Takahashi, I., Ishibashi, F., Furuhama, S., Kai, R., and Sato, M., “Oil Film Thickness Measurement and Analysis of a Three Ring Pack in an Operating Diesel Engine,” SAE Technical Paper 2000-01-1787, 2000, doi.org/10.4271/2000-01-1787.

[7] Dhar, A., Agarwal, A., and Saxena, V., “Measurement of Lubricating Oil Film Thickness between Piston Ring-liner Interface in an Engine Simulator,” SAE Technical Paper 2008-28-0071, 2008, doi.org/10.4271/2008-28-0071.

[8] Dhar, A., Argarwal, A., and Saxena, V., “Measurement of dynamic lubricating oil film thickness between piston ring and liner in a motored engine,” *Sensors and Actuators A: Phsysical* 149, no. 1 (2009): 7-15, doi:10.1016/j.sna.2008.09.021

[9] Sherrington, I., and Smith, E,. “Experimental methods for measuring the oil-film thickness between the piston-rings and cylinder-wall of internal combustion engines,” *Tribology International* 18, no. 6 (1985): 315-320, doi:10.1016/0301-679X(85)90077-5

[10] Garcia-Atance Fatjo, G., Smith, E., and Sherrington, I., “Mapping lubricating film thickness, film extent and ring twist for the compression-ring in a firing internal combustion engine,” *Tribology International* 70 (2014): 112-118, https://doi.org/10.1016/j.triboint.2013.10.001.

[11] Garcia-Atance Fatjo, G., Smith, E., and Sherrington, I. “Piston-ring film thickness: Theory and experiment compared,” *Proceedings of the Institution of Mechanical Engineers, Part J: Journal of Engineering Tribology* 232, no. 5 (2018): 550-567, doi:10.1177/1350650117722257.

[12] Söchting, S., and Sherrington, I., “The effect of load and viscosity on the minimum operating oil film thickness of piston-rings in internal combustion engines,” *Proceedings of the Institution of Mechanical Engineers, Part J: Journal of Engineering Tribology* 233, no. 3 (2009): 383-391, doi:10.1243/13506501JET556.

[13] Takiguchi, M., Nakayama, K., Furuhama, S., and Yoshida, H., "Variation of Piston Ring Oil Film Thickness in an Internal Combustion Engine – Comparison Between Thrust and Anti-Thrust Sides," SAE Technical Paper 980563, 1998, doi:10.4271/980563.

[14] Seki, T., Nakayama, K., Yamada, T., Yoshida, A., et al., "A study on variation in oil film thickness of a piston ring package: variation of oil film thickness in piston sliding direction," *JSAE Review* 21 no. 3 (2000): 315-320 doi:10.1016/S0389-4304(00)00044-8.

[15] Notay, R., Priest, M., and Fox, M., "The influence of lubricant degradation on measured piston ring film thickness in a fired gasoline reciprocating engine," *Tribology International* 129 (2019) 112-123 doi:10.1016/j.triboint.2018.07.002.

[16] Baba, Y., Suzuki, H., Sakai, Y., Teck Wei, D., et al., "PIV/LIF Measurement of Oil Film Behavior on the Piston I. C. Engine," SAE Technical Paper 2007-24-0001, 2007, doi:10.4271/2007-24-0001.

[17] Ting, L. "Development of a laser fluorescence technique for measuring piston ring oil film thickness," *Journal of Tribology* 102, no. 2 (1980): 165-170 doi:10.1115/1.3251458.

[18] Taylor, R., and Evans, P., "In-situ piston measurements," *Proceedings of the Institution of Mechanical Engineers, Part J: Journal of Engineering Tribology* 218 no. 3 (2004): 185-200 doi:10.1243/1350650041323386.

[19] Saad, P., Kamo, L., Mekari, M., Bryzik, W., et al., "Modeling and measurement of tribological parameters between piston rings-liner in turbocharged diesel engine," SAE Technical Paper 2007-01-1440, 2007, doi:10.1115/ijtc2006-12308.

[20] Bulsara, M., Bhatt, D., and Mistry, K., "Measurement of oil film thickness between piston ring and liner using strain guage," *Industrial Lubrication and Tribology* 65 no. 5 (2013): 297-304 doi:10.1108/ILT-02-2011-0013.

[21] Tamminen, J., Sandtröm, C., and Andresson, P., "Influence of load on the tribological conditions in piston ring and cylinder liner contacts in a medium-speed diesel engine," *Tribology International* 39 no. 12 (2006): 1643-1652 doi: 10.1016/j.triboint.2006.04.003.

[22] Dow, T., Schiele, C., and Stockwell, R., "Technique for Experimental Evaluation of Piston Ring-Cylinder Film Thickness," *Journal of Lubrication Technology* 105 no. 3 (1983): 353-360 doi.org/10.1115/1.3254608.

[23] Avan, E., Mills, R., and Dwyer-Joyce, R., "Ultrasonic imaging of the piston ring oil film during operation in a motored engine – Towards oil film thickness measurement," SAE Technical Paper 2010-01-2179, 2010, doi:10.4271/2010-01-2179.

[24] Mills, R., "Ultrasonic measurement of lubricant films generated at the piston-cylinder interface of internal combustion engines," PhD Thesis, University of Sheffield, 2012.

[25] Mills, R. Vail, J., and Dwyer-Joyce, R., "Ultrasound for the non-invasive measurement of internal combustion engine piston ring oil films," *Proceedings of the Institution of Mechanical Engineers, Part J: Journal of Engineering Tribology* 229 no. 2 (2015): 207-215 doi:10.1177/1350650114552538.

[26] Mills, R., Avan, E., and Dwyer-Joyce, R., "Piezoelectric sensors to monitor lubricant film thickness at piston-cylinder contacts in a fired engine," *Proceedings of the Institution of Mechanical Engineers, Part J: Journal of Engineering Tribology* 227 no. 2 (2013): 100-111 doi:10.1177/1350650112464833.

[27] Mills, R., and Dwyer-Joyce, R., “Ultrasound for the non-invasive measurement of IC engine piston skirt lubricant films,” Proceedings of the Institution of Mechanical Engineers, Part J: Journal of Engineering Tribology 228 no. 11 (2014): 1330-1340 doi:10.1177/1350650114538616.

[28] Dwyer-Joyce, R., Green, D., Harper, P., Lewis, R., et al., “The measurement of liner – Piston skirt oil film thickness by an ultrasonic means,” SAE Technical Paper 2006-01-0648 , 2006, doi:10.4271/2006-01-0648.

[29] Stark, M., and Mittler, R., “Optimization of Tribodynamic Effects to Improve the Reduction Potential of Particulate Matter Concentrations in the Exhaust Gas of Large Two Stroke Marine Diesel Engines,” *SAE International Journal of Fuels and Lubricants* 7 no. 3 (2014): 965-978 doi:10.4271/2014-01-2844.

[30] Schoenberg, M., “Elastic wave behavior across linear slip interfaces,” *Journal of the Acoustical Society of America* 65 no. 5 (1980): 1516-1521 doi:10.1121/1.385077.

[31] Dwyer-Joyce, R., Drinkwater, B., Donohoe, C., “The measurement of lubricant-film thickness using ultrasound,” *Proceedings of the Royal Society A: Mathematical, Physical and Engineering Sciences* 459 no. 2032 (2003): 957-976 doi:10.1098/rspa.2002.1018.

[32] Nicholas, G., Howard, T., Long, H., Wheals, J., et al., “Measurement of roller load, load variation, and lubrication in a wind turbine gearbox high speed shaft bearing in the field,” *Tribology International* 148 (2020) doi:10.1016/j.triboint.2020.106322.

[33] Howard, T., “Development of a Novel Bearing Concept for Improved Wind Turbine Gearbox Reliability,” PhD Thesis, University of Sheffield, 2016.

[34] Hunter, A., “Ultrasonic Measurements of the Strip Thickness, Lubricant Film, Thickness, Roll Deflection and Roll Stress in the Roll Bite in the Cold Rolling of Steel,” PhD Thesis, University of Sheffield, 2018.